Journal of Sound and Vibration (1999) **225**(4), 655–699
Article No. jsvi.1999.2255, available online at http://www.idealibrary.com on IDEAL®

NON-LINEAR DYNAMICS AND STABILITY OF CIRCULAR CYLINDRICAL SHELLS CONTAINING FLOWING FLUID. PART I: STABILITY

M. AMABILI

Dipartimento di Ingegneria Industriale, Università di Parma, Viale delle Scienze, Parma, I - 43100 Italy

F. PELLICANO

Dipartimento di Scienze dell'Ingegneria, Università di Modena, Via Campi 213b, Modena, I - 41100 Italy

AND

M. P. PAÏDOUSSIS

Department of Mechanical Engineering, McGill University, 817 Sherbrooke Street W., Montreal, Québec, Canada H3A 2K6

(*Received* 1 *October* 1998, *and in final form* 8 *February* 1999)

The study presented is an investigation of the non-linear dynamics and stability of simply supported, circular cylindrical shells containing inviscid incompressible fluid flow. Non-linearities due to large-amplitude shell motion are considered by using the non-linear Donnell's shallow shell theory, with account taken of the effect of viscous structural damping. Linear potential flow theory is applied to describe the fluid–structure interaction. The system is discretiszd by Galerkin's method, and is investigated by using a model involving seven degrees of freedom, allowing for travelling wave response of the shell and shell axisymmetric contraction. Two different boundary conditions are applied to the fluid flow beyond the shell, corresponding to: (i) infinite baffles (rigid extensions of the shell), and (ii) connection with a flexible wall of infinite extent in the longitudinal direction, permitting solution by separation of variables; they give two different kinds of dynamical behaviour of the system, as a consequence of the fact that axisymmetric contraction, responsible for the softening non-linear dynamical behaviour of shells, is not allowed if the fluid flow beyond the shell is constrained by rigid baffles. Results show that the system loses stability by divergence.

1. INTRODUCTION

Several studies have been conducted todate on the dynamic stability of circular cylindrical shells subjected to either internal or external axial flow. Particularly interesting, in the case of internal flow, are the studies of Païdoussis and Denise [1],

0022-460X/99/340655 + 45 $30.00/0

Weaver and Unny [2], Matsuzaki and Fung [3] and Païdoussis *et al.* [4]. In all of this work, the analysis is linear, and fluid flow is modelled by potential flow theory.

Païdoussis and Denise [1] considered both clamped and cantilevered shells and utilized a travelling-wave-type solution, nevertheless satisfying the pertinent boundary conditions, along with a separation of variables method to solve the boundary value problem for the fluid–structure interaction. Weaver and Unny [2], on the other hand, investigated the linear stability of simply supported shells by means of the Fourier transform method to solve the fluid–structure interaction. In both references [1, 2], damping was neglected; however, it was included in the analysis by Matsuzaki and Fung [3], who showed that post-divergence coupled-mode flutter of the simply supported system is not possible. Païdoussis *et al.* [4] extended this study to shells in annular flow, and for both internal and annular flow extended the analysis further to deal with a viscous fluid flow [5]. Although viscous effects can be extremely important for annular flows, it was shown that for internal flow they are much less so, which is of particular importance in the present study where the flow is assumed to be inviscid.

Non-linear flutter of flat and curved plates ("panels"), e.g., see references [6–10], and beams (pipes), e.g., see reference [11], has been studied extensively. In contrast, non-linear studies of shells subjected to internal or external axial flow are few. The first one appears to be by Olson and Fung [12]. They modelled simply supported shells using Donnell's non-linear shallow shell theory, using a two-mode expansion without considering the companion mode (second standing-wave mode, the orientation of which is at $\pi/(2n)$ with respect to the previous one, n being the number of nodal diameters). In their study, the fluid flow is external to the shell and supersonic, and it is modelled by using linear piston theory. In subsequent studies, Evensen and Olson [13, 14] considered also the companion mode, therefore employing a four-degree-of-freedom mode expansion. This expansion allows the study of travelling-wave-mode flutter, where nodal lines are travelling circumferentially around the shell; this phenomenon is similar to travelling waves predicted and measured for large-amplitude forced vibrations of shells [15–18]. However, similarly to Evensen's [15] expansion, these expansions are not moment-free at the ends of the shell, as they should be for classical simply supported shells, and the homogeneous solution for the stress function is neglected. Evensen and Olson investigated periodic solutions by using the harmonic balance method and solved the non-linear algebraic equations for some special cases. Olsson [19] added to the problem the effect of a particular temperature field.

Lakis and Laveau [20] studied the non-linear vibrations of anisotropic circular cylindrical shells containing a flowing fluid by using a hybrid finite element method. In this study, Sanders' linear shell theory is used and the non-linearities retained are due only to the fluid flow, which is described by potential flow theory; specifically, the Bernoulli equation was expanded to second order and a linear boundary condition was used to satisfy the impermeability condition at the fluid–shell interface. Results show that this kind of fluid non-linearity can be neglected for all the vibration amplitudes of physical significance. This confirms the Evensen and

Olson [13, 14] findings. Again, this is particularly important to the present study, where, although shell motions are described by non-linear shell theory, linear potential flow theory is retained for modelling the fluid motions.

Selmane and Lakis [21] considered the non-linear vibrations of open and closed circular cylindrical shells† with fluid flow by using a hybrid finite element method. In contrast to the previous study, the non-linear Sanders–Koiter shell theory is used, so that structural non-linearities are taken into account, but the fluid–structure boundary condition is still expressed by a linear relation. Results show only the effect of vibration amplitude on vibration frequencies. It is found that non-linearity produces either hardening or softening behaviour in open circular cylindrical shells, depending on the circumferential wave number n, for both quiescent and flowing fluid. This is different to what has been found in other theoretical and experimental studies on non-linear shell vibration, e.g., for closed circular cylindrical shells, Evensen [15], Chen and Babcock [17], Gonçalves and Batista [22], Ganapathi and Varadan [23] and Amabili *et al.* [18] in all of which a softening-type non-linearity is predicted. Furthermore, studies available for open circular cylindrical shell *in vacuo* also indicate a softening behaviour (see reference [18] for other references). No results are presented by Selmane and Lakis [21] for closed circular cylindrical shells with flowing fluid, and the response of a shell and its stability are not investigated, nor are companion mode participation and the effect of structural damping considered (actually only the backbone curve, pertaining to free vibrations, is obtained).

A full literature review of work on the non-linear dynamics of shells *in vacuo* and filled with or surrounded by quiescent fluid has been given by Amabili *et al.* [18] and will not be repeated here. One important conclusion reached in that study, however, is the following. Since most analyses involve some kind of Galerkin-type expansion, the choice of appropriate comparison functions is as always important, but in the case of non-linear shell motions it is *crucial*; a linear modal base is the simplest and best choice. Furthermore, in order to reduce the number of degrees of freedom, it is important to use only the most significant modes. Thus, in addition to representing both the regular or "driven" asymmetric modes and the "companion modes", it is important to also include axisymmetric modes. This is because it has clearly been established that, for non-linear shell motions, the deformation of the shell involves a small but important axisymmetric contraction of the circumference. This is important in predicting the kind of softening behaviour that has been observed in the experiments (e.g. see reference [17]).

The present study seems to be the first one on the non-linear dynamics and stability of circular cylindrical shells containing fluid flow. It is aimed at clarifying several aspects of the dynamics and stability of simply supported shells subjected to internal flow that linear studies were unable to investigate. Linear potential flow theory is applied to describe the fluid–structure interaction; in fact, the amplitude of shell displacements remains small enough for linear fluid mechanics to be adequate.

†Closed in the sense that the circumference is closed, in contrast to a shell with an open, incomplete circular cross-section.

In contrast, the non-linearities due to large amplitude shell motion[†] are taken into account by using Donnell's non-linear shallow shell theory. The effect of viscous structural damping is retained in the present study. The system is discretized by Galerkin's method, and is investigated by using a low-dimensional model involving seven degrees of freedom, allowing for the travelling wave response around the shell. Two different sets of boundary conditions are applied to the fluid flow beyond the shell extremities, corresponding to (i) infinite baffles (rigid extensions of the shell) and (ii) connection with a flexible wall of infinite extent in the longitudinal direction, permitting solution by separation of variables. They give two entirely different kinds of dynamical behaviour of the system, as a consequence of the fact that axisymmetric contraction, responsible for the softening behaviour of shells, is not possible if the fluid flow beyond the shell is constrained by infinite rigid baffles (since this hypothesis would imply an infinite kinetic energy for the fluid). Numerical results show that the system loses stability by divergence.

2. NON-LINEAR MODEL OF THE SHELL

In this study, attention is focused on both a finite, simply supported, closed circular cylindrical shell of length L, and an infinitely long shell, periodically supported. In the last case, the portion of the shell considered lies between two supports, L apart, while the effect of the part of the shell beyond this length is only considered as a constraint; only modes that are antisymmetric with respect to each support are considered in this case (lower frequency modes). A cylindrical co-ordinate system (O; x, r, θ) is chosen, with the origin O placed at the centre of one end of the shell. The displacements of points in the middle surface of the shell are denoted by u, v and w, in the axial, circumferential and radial direction respectively. Using Donnell's shallow-shell non-linear theory, gives the equation of motion for large amplitude transverse vibrations of a very thin, circular cylindrical shell as [15, 17]

$$D\nabla^4 w + ch\dot{w} + \rho h\ddot{w} = f - p + \frac{1}{R}\frac{\partial^2 F}{\partial x^2} + \left(\frac{\partial^2 F}{R^2\partial\theta^2}\frac{\partial^2 w}{\partial x^2} - 2\frac{\partial^2 F}{R\,\partial x\partial\theta}\frac{\partial^2 w}{R\,\partial x\partial\theta} + \frac{\partial^2 F}{\partial x^2}\frac{\partial^2 w}{R^2\partial\theta^2}\right), \quad (1)$$

where $D = Eh^3/[12(1-\nu^2)]$ is the flexural rigidity, E is Young's modulus, ν is Poisson's ratio, h the shell thickness, R the mean shell radius, ρ the mass density of the shell, c (kg/m^3 s) the damping coefficient, and f and p are the radial pressures applied to the surface of the shell as a consequence of external forces and the contained flowing fluid respectively[‡] The radial deflection w is positive inward,

[†]A few words to define "large" are useful. In the context of shell theory, large amplitudes signify amplitudes exceeding the shell thickness, or of several times the shell thickness, which in other contexts may be still considered to be small.

[‡]In this paper, in the calculations presented in section 6, $f = 0$ is taken throughout.

$\dot{w} = (\partial w/\partial t)$, $\ddot{w} = (\partial^2 w/\partial t^2)$ and F is the in-plane stress function; F is given by [15, 17]

$$\frac{1}{Eh}\nabla^4 F = -\frac{1}{R}\frac{\partial^2 w}{\partial x^2} + \left[\left(\frac{\partial^2 w}{R\partial x\partial\theta}\right)^2 - \frac{\partial^2 w}{\partial x^2}\frac{\partial^2 w}{R^2\partial\theta^2}\right]. \tag{2}$$

In equations (1) and (2), the biharmonic operator is defined as $\nabla^4 = [\partial^2/\partial x^2 + \partial^2/(R^2\partial\theta^2)]^2$. These equations are based on Donnell's nonlinear shallow-shell theory, so that the results are accurate only for modes of high circumferential wavenumber n (n is the number of nodal diameters); specifically, $1/n^2 \ll 1$ must be satisfied, so that $n \geqslant 5$ is required in order to have fairly good accuracy. Donnell's non-linear shallow-shell theory is obtained by neglecting the in-plane inertia, transverse shear deformation and rotary inertia, so that it gives accurate results only for very thin shells, i.e., $h \ll R$; the predominant non-linear terms are retained but other secondary effects, such as the non-linearities in curvature strains, have been neglected.

The forces per unit length in the axial and circumferential directions, as well as the shear force, are given by [24, 25]

$$N_x = \frac{1}{R^2}\frac{\partial^2 F}{\partial\theta^2}, \qquad N_\theta = \frac{\partial^2 F}{\partial x^2}, \qquad N_{x\theta} = -\frac{1}{R}\frac{\partial^2 F}{\partial x\partial\theta}. \tag{3}$$

The strain–displacement relations are [24, 25]

$$(1-\nu^2)\frac{N_x}{Eh} = -\frac{\nu w}{R} + \frac{1}{2}\left(\frac{\partial w}{\partial x}\right)^2 + \frac{\nu}{2}\left(\frac{\partial w}{R\partial\theta}\right)^2 + \frac{\partial u}{\partial x} + \frac{\nu}{R}\frac{\partial v}{\partial\theta}, \tag{4}$$

$$(1-\nu^2)\frac{N_\theta}{Eh} = -\frac{w}{R} + \frac{\nu}{2}\left(\frac{\partial w}{\partial x}\right)^2 + \frac{1}{2}\left(\frac{\partial w}{R\partial\theta}\right)^2 + \nu\frac{\partial u}{\partial x} + \frac{1}{R}\frac{\partial v}{\partial\theta}, \tag{5}$$

$$(1-\nu^2)\frac{N_{x\theta}}{Eh} = 2(1-\nu)\left[\frac{1}{R}\frac{\partial w}{\partial x}\frac{\partial w}{\partial\theta} + \frac{1}{R}\frac{\partial u}{\partial\theta} + \frac{\partial v}{\partial x}\right]. \tag{6}$$

The flexural deformation w is expanded by using the linear shell eigenmodes as basis; in particular, the flexural response having n nodal diameters and m longitudinal half-waves can be written as

$$w(x,\theta,t) = \sum_{m=1}^{N_1}[A_{m,n}(t)\cos(n\theta) + B_{m,n}(t)\sin(n\theta)]\sin(\lambda_m x) + \sum_{m=1}^{N_2} A_{m,0}(t)\sin(\lambda_m x), \tag{7a}$$

where $\lambda_m = m\pi/L$ and t is the time; $A_{m,n}(t)$, $B_{m,n}(t)$ and $A_{m,0}(t)$ are unknown functions of t. Equation (7a) was obtained by supposing that the non-linear interaction among linear modes of the chosen basis involves only the asymmetric modes ($n > 0$) having a given n value, and all the axisymmetric modes ($n = 0$);

therefore, only the non-linear interaction among asymmetric modes of different n is neglected. Axisymmetric modes play an important role in non-linear vibrations, as pointed out in the Introduction, and the interaction between asymmetric modes of the same n is fundamental in the investigation of stability in the case of a flowing fluid. This is the reason why they are included in the present low-dimensional model. In the following analysis, the sums in equation (7a) are truncated at $N_1 = 2$ and $N_2 = 5$. Axisymmetric modes having an even m value can be eliminated in the expansion, because they do not contribute to shell contraction. In fact, they present an integer number of longitudinal waves and therefore they have an average deflection equal to zero on the shell length. In other words, at any instant along the shell there is a number $m/2$ of half-waves moving inwards and $m/2$ moving outwards, giving zero average contraction (in case of vibration considering only the asymmetric mode with $m = 1$; axisymmetric modes having an even m value can be eliminated for symmetry reasons). Specifically, the following mode expansion is used:

$$w(x, \theta, t) = \sum_{m=1}^{2} [A_{m,n}(t) \cos(n\theta) + B_{m,n}(t) \sin(n\theta)] \sin(\lambda_m x) + \sum_{m=1}^{3} A_{(2m-1),0}(t) \sin(\lambda_{(2m-1)} x). \tag{7b}$$

The mode expansion of equation (7b) may be considered as a more sophisticated version of that used by Amabili *et al.* [18] where sums were truncated to $N_1 = 1$ and $N_2 = 3$, since only modes with $m = 1$ were investigated in that study. Equation (7b) satisfies the boundary conditions

$$w = 0 \quad \text{and} \quad M_x = -D\{(\partial^2 w/\partial x^2) + v[\partial^2 w/(R^2 \partial \theta^2)]\} = 0 \quad \text{at } x = 0, L, \tag{8}$$

where M_x is the bending moment per unit length. The other boundary conditions differ for the simply supported shell of finite length (case 1) and for the infinitely long, periodically supported shell with restrained axial displacement at the supports (case 2). They are as follows:

$$\text{Case 1:} \quad N_x = 0 \text{ at } x = 0, L \text{ and } v = 0 \text{ at } x = 0, L, \tag{9a}$$

$$\text{Case 2:} \quad u = 0 \text{ at } x = 0, L \text{ and } v = 0 \text{ at } x = 0, L; \tag{9b}$$

moreover, u, v and w must be continuous in θ. Case 1 corresponds to the classical simply supported shell. The conditions imposed in case 2 are well justified by the reciprocal constraint between the part of the shell under consideration and extensions thereof outside (0, L). Case 2 also approximates a shell with rings at the ends. By using the present formulation, it is also possible to study a shell subjected to axisymmetric prestress, i.e., $N_x = \tilde{N}_x$ and $N_\theta = \tilde{N}_\theta$ at $x = 0, L$.

3. HYDRODYNAMIC LOADING

In the present study, non-linearities are attributed to the shell dynamics, but the fluid–structure interaction is described by linear potential flow theory. Evensen and

Olson [13, 14] observed that the flutter amplitudes remain within the linear range from the aerodynamics point of view. The non-linear effects in the dynamic pressure and in the boundary conditions at the fluid–structure interface have been found to be negligible by Gonçalves and Batista [22], Ginsberg [26] and Lakis and Laveau [20] in the case of quiescent fluids.

The fluid flow is internal to the shell. The fluid is assumed to be incompressible and inviscid, and the flow to be isentropic and irrotational. Gravity effects, such as prestress in the shell due to the fluid weight, are neglected. The irrotationality property is the condition for the existence of a scalar potential function Ψ from which the velocity may be written as

$$\mathbf{v} = -\nabla\Psi. \tag{10}$$

The potential Ψ consists of two components: one due to the mean flow associated with the undisturbed flow velocity U in the axial direction, and the unsteady component Φ associated with the shell motion. Thus

$$\Psi = -Ux + \Phi. \tag{11}$$

The potential of the unsteady component Φ satisfies the Laplace equation

$$\nabla^2\Phi = \frac{\partial^2\Phi}{\partial x^2} + \frac{\partial^2\Phi}{\partial r^2} + \frac{1}{r}\frac{\partial\Phi}{\partial r} + \frac{1}{r^2}\frac{\partial^2\Phi}{\partial\theta^2} = 0. \tag{12}$$

The perturbed pressure P may be related to the velocity potential by Bernoulli's equation for unsteady fluid flow,

$$-\frac{\partial\Phi}{\partial t} + \frac{1}{2}V^2 + \frac{P}{\rho} = \frac{P_S}{\rho}, \tag{13}$$

where $V^2 = \nabla\Psi\cdot\nabla\Psi$, P_S is the stagnation pressure and ρ_F is the fluid mass density. The pressure P in the fluid domain can be written as

$$P = \bar{P} + p,$$

where $\bar{P}$ is the mean pressure and p is the perturbation pressure. For small perturbations, $V^2 \simeq U^2 - 2U(\partial\Phi/\partial x)$, and equation (13) gives the stagnation pressure $P_S = \bar{P} + \frac{1}{2}\rho_F U^2$, so that it is fixed for an assumed mean flow velocity and its effect on shell dynamics is neglected. Then, equation (13) gives the following expression for the perturbation pressure:

$$p = \rho_F\left(\frac{\partial\Phi}{\partial t} + U\frac{\partial\Phi}{\partial x}\right). \tag{14}$$

3.1. THE WEAVER AND UNNY MODEL

Initially, the model introduced by Randall [27] and specialized by Weaver and Unny [2] to shells containing flowing fluid is considered. In this case, rigid baffles

(extensions), of the same internal diameter as the shell, limit the fluid domain; these baffles are indefinitely long in the axial direction and are connected to the shell, one at $x = 0$ and the other at $x = L$. Axisymmetric modes ($n = 0$) of the shell are no longer possible when using this model, because they would result in an infinite kinetic energy of the fluid and hence, they must be eliminated in the expansion of w. This item will be discussed further later in this section.

Upon assuming no cavitation, the boundary condition on the fluid-shell interface is

$$\left(\frac{\partial \Phi}{\partial r}\right)_{r=R} = \begin{cases} \left(\dfrac{\partial w}{\partial t} + U\,\dfrac{\partial w}{\partial x}\right) & \text{for } 0 \leqslant x \leqslant L, \\ 0 & \text{for } x < 0 \text{ and } x > L. \end{cases} \tag{15}$$

Upon assuming $w = A(t)\sin(m\pi x/L)\cos(n\theta)$ and noting that all the terms in the assumed mode expansion of w may be written in similar form, Φ may be written as

$$\Phi = \psi_n(x, r, t)\cos(n\theta). \tag{16}$$

In order to solve the mixed boundary value problem, it is useful to introduce the Fourier transform

$$\psi_n^* = \int_{-\infty}^{\infty} \psi_n(x, r, t)\,\mathrm{e}^{-j\alpha x}\,\mathrm{d}x, \tag{17}$$

where $j = \sqrt{-1}$ and in which the following conditions have been used:

$$\lim_{x \to \pm\infty} \psi_n(x, r, t) = 0 \quad \text{and} \quad \lim_{x \to \pm\infty} \frac{\partial \psi_n}{\partial x} = 0;$$

α is the Fourier transform variable. By using equations (16) and (17), the Laplace equation becomes

$$r^2\,\frac{\partial^2 \psi_n^*}{\partial r^2} + r\,\frac{\partial \psi_n^*}{\partial r} - (n^2 + \alpha^2 r^2)\psi_n^* = 0. \tag{18}$$

The solution of equation (18) which is regular at $r = 0$ has the form

$$\psi_n^*(\alpha, r, t) = c_n(\alpha, t)\mathrm{I}_n(\alpha r), \tag{19}$$

where I_n is the modified Bessel function of order n, and I_n' is its derivative with respect to the argument. By using equation (19), equation (15) yields

$$\alpha\, c_n(\alpha, t)\mathrm{I}_n'(\alpha R) = \int_0^L [\sin(m\pi x/L)\,\dot{A}(t) + U(m\pi/L)\cos(m\pi x/L)\,A(t)]\,\mathrm{e}^{-j\alpha x}\,\mathrm{d}x$$

$$= \frac{mL\pi[1 - (-1)^m\,\mathrm{e}^{-j\alpha L}]}{m^2\pi^2 - \alpha^2 L^2}\,[\dot{A}(t) + j\alpha U\,A(t)]. \tag{20}$$

Equations (19) and (20) give

$$\psi_n^*(\alpha, r, t) = \frac{mL\pi[1 - (-1)^m \mathrm{e}^{-j\alpha L}]}{m^2\pi^2 - \alpha^2 L^2} \frac{\mathrm{I}_n(\alpha r)}{\alpha \mathrm{I}_n'(\alpha R)} [\dot{A}(t) + j\alpha U A(t)]. \tag{21}$$

The inverse Fourier transform gives

$$\psi_n(x, r, t) = \frac{1}{2\pi} \int_{-\infty}^{\infty} \psi_n^*(\alpha, r, t) \mathrm{e}^{j\alpha x} \, \mathrm{d}\alpha. \tag{22}$$

Equation (22) gives a finite result only for $n \neq 0$. In fact, axisymmetric modes ($n = 0$) having an odd number m of axial half-waves are associated with the motion of an infinite fluid volume; hence, they are physically impossible. Therefore, axisymmetric modes must not be included in the mode expansion, equation (7), if infinite rigid baffles are considered beyond the axial limits of the shell.

For the perturbation pressure, it is possible to write

$$p = p_n \cos(n\theta). \tag{23}$$

It is useful to apply the Fourier transform in this case also,

$$p_n^*(\alpha, r, t) = \int_{-\infty}^{\infty} p_n(x, r, t) \mathrm{e}^{-j\alpha x} \, \mathrm{d}x. \tag{24}$$

In the transformed domain, by using equation (14), it is possible to write

$$\begin{aligned}(p_n^*)_{r=R} &= \rho_F \left(\frac{\partial \psi_n^*}{\partial t} + \mathrm{j}\alpha U \psi_n^* \right)_{r=R} \\ &= \rho_F \frac{mL\pi[1 - (-1)^m \mathrm{e}^{-j\alpha L}]}{m^2\pi^2 - \alpha^2 L^2} \frac{\mathrm{I}_n(\alpha R)}{\alpha \mathrm{I}_n'(\alpha R)} [\ddot{A}(t) + 2\mathrm{j}\alpha U \dot{A}(t) - \alpha^2 U^2 A(t)].\end{aligned} \tag{25}$$

Finally, the perturbation pressure at the shell wall that appears in equation (1) is given by

$$\begin{aligned}p_{r=R} = \rho_F \frac{L}{2} \cos(n\theta) \int_{-\infty}^{\infty} &\frac{m[1 - (-1)^m \mathrm{e}^{-j\alpha L}]}{m^2\pi^2 - \alpha^2 L^2} \frac{\mathrm{I}_n(\alpha R)}{\alpha \mathrm{I}_n'(\alpha R)} \\ &\times [\ddot{A}(t) + 2\mathrm{j}\alpha U \dot{A}(t) - \alpha^2 U^2 A(t)] \mathrm{e}^{j\alpha x} \, \mathrm{d}\alpha.\end{aligned} \tag{26}$$

3.2. THE PAÏDOUSSIS AND DENISE MODEL

In this case, the fluid domain is a cylinder of infinite extent, within a periodically supported shell of infinite length, so that it is possible to employ the method of separation of variables to obtain the velocity potential. Here the mathematical trick is to consider the function w and the fluid domain defined for any $x \in (-\infty, \infty)$. This means that w is a periodic function with main period $2L$, and the same is verified for the velocity potential and the perturbation pressure. This type of

solution was initially introduced by Niordson [28] and then used by Païdoussis and Denise [1].

If there is no cavitation at the fluid–shell interface, one can write

$$\left(\frac{\partial \Phi}{\partial r}\right)_{r=R} = \left(\frac{\partial w}{\partial t} + U\,\frac{\partial w}{\partial x}\right). \tag{27}$$

By using the method of separation of variables, the function Φ may be written as

$$\Phi(x, r, \theta, t) = \phi(x)\psi(r)\cos(n\theta) f(t). \tag{28}$$

Substituting equation (28) into equation (12) and using the condition that the velocity potential must be regular at $r = 0$, one finds that

$$\psi(r) = c\,\mathrm{I}_n(m\pi r/L). \tag{29}$$

Equation (27) is then satisfied by taking

$$\Phi = \frac{L}{m\pi}\,\frac{\mathrm{I}_n(m\pi r/L)}{\mathrm{I}'_n(m\pi R/L)}\left(\frac{\partial w}{\partial t} + U\,\frac{\partial w}{\partial x}\right), \tag{30}$$

where w is given by equation (7b) and is therefore of the generic form $w = A(t)\sin(m\pi x/L)\cos(n\theta)$. The perturbation pressure at the shell wall, by using equation (14), is given by

$$p_{r=R} = \rho_F\,\frac{L}{m\pi}\,\frac{\mathrm{I}_n(m\pi R/L)}{\mathrm{I}'_n(m\pi R/L)}\left(\frac{\partial}{\partial t} + U\,\frac{\partial}{\partial x}\right)^2 w. \tag{31}$$

4. REDUCTION TO A FINITE-DIMENSIONAL MODEL

Substituting the expansion of w, equation (7b), on the right-hand side of equation (2) yields a partial differential equation for the stress function F, the solution of which may be written as

$$F = F_h + F_p, \tag{32}$$

where F_h is the homogeneous and F_p is the particular solution. The particular solution is given by

$$\begin{aligned} F_p = {} & c_1(t)\cos(n\theta)\sin(\pi x/L) + c_2(t)\sin(n\theta)\sin(\pi x/L) + c_3(t)\cos(n\theta)\sin(2\pi x/L) \\ & + c_4(t)\sin(n\theta)\sin(2\pi x/L) + c_5(t)\sin(\pi x/L) + c_6(t)\sin(3\pi x/L) \\ & + c_7(t)\sin(5\pi x/L) + c_8(t)\cos(\pi x/L) + c_9(t)\cos(2\pi x/L) + c_{10}(t)\cos(3\pi x/L) \\ & + c_{11}(t)\cos(4\pi x/L) + c_{12}(t)\cos(n\theta) + c_{13}(t)\cos(n\theta)\cos(\pi x/L) \end{aligned}$$

$$+ c_{14}(t)\cos(n\theta)\cos(2\pi x/L) + c_{15}(t)\cos(n\theta)\cos(3\pi x/L)$$

$$+ c_{16}(t)\cos(n\theta)\cos(4\pi x/L) + c_{17}(t)\cos(n\theta)\cos(5\pi x/L)$$

$$+ c_{18}(t)\cos(n\theta)\cos(6\pi x/L) + c_{19}(t)\cos(n\theta)\cos(7\pi x/L) + c_{20}(t)\sin(n\theta)$$

$$+ c_{21}(t)\sin(n\theta)\cos(\pi x/L) + c_{22}(t)\sin(n\theta)\cos(2\pi x/L)$$

$$+ c_{23}(t)\sin(n\theta)\cos(3\pi x/L) + c_{24}(t)\sin(n\theta)\cos(4\pi x/L)$$

$$+ c_{25}(t)\sin(n\theta)\cos(5\pi x/L) + c_{26}(t)\sin(n\theta)\cos(6\pi x/L)$$

$$+ c_{27}(t)\sin(n\theta)\cos(7\pi x/L) + c_{28}(t)\cos(2n\theta)$$

$$+ c_{29}(t)\cos(2n\theta)\cos(\pi x/L) + c_{30}(t)\cos(2n\theta)\cos(3\pi x/L) + c_{31}(t)\sin(2n\theta)$$

$$+ c_{32}(t)\sin(2n\theta)\cos(\pi x/L) + c_{33}(t)\sin(2n\theta)\cos(3\pi x/L), \tag{33}$$

where the functions c_i , $i = 1, \ldots, 33$, are given in Appendix A.

The expansion used for the transverse displacement w satisfies the boundary conditions given by equations (8); moreover, it satisfies exactly the continuity of circumferential displacement, as shown in Appendix B. The boundary conditions for either of the in-plane displacements, equations (9), are satisfied on average. Specifically, the following conditions are imposed:

$$\int_0^{2\pi} N_x R \, \mathrm{d}\theta = 0, \quad \text{case 1,} \tag{34a}$$

$$\int_0^{2\pi} \int_0^L \frac{\partial u}{\partial x} \, \mathrm{d}x R \, \mathrm{d}\theta = \int_0^{2\pi} [u(L, \theta) - u(0, \theta)] R \, \mathrm{d}\theta = 0, \quad \text{case 2,} \tag{34b}$$

and for both cases

$$\int_0^{2\pi} \int_0^L N_{x\theta} \, \mathrm{d}x R \, \mathrm{d}\theta = 0. \tag{35}$$

Equation (34a) assures a zero axial force N_x on the average, while equation (34b) states that the axial displacement u is zero on average at $x = 0, L$. Equation (35) is satisfied when u and w are continuous in θ on average, and $v = 0$ on average at $x = 0, L$. Substitution of equation (9) with equations (34) and (35) simplifies computations, but on the other hand it introduces an approximation. A similar approach has been used widely in the past in the study of non-linear vibrations of shells; see, e.g., references [18, 24, 25].

The homogeneous solution of equation (2) may be assumed to be of the form [18]

$$F_h = \frac{1}{2}\bar{N}_x R^2\theta^2 + \frac{1}{2}x^2\left\{\bar{N}_\theta - \frac{1}{2\pi RL}\int_0^L\int_0^{2\pi}\left[\frac{\partial^2 F_p}{\partial x^2}\right]R\,\mathrm{d}\theta\,\mathrm{d}x\right\} - \bar{N}_{x\theta}xR\theta$$

$$= \frac{1}{2}\bar{N}_x R^2\theta^2 + \frac{1}{2}x^2\left\{\bar{N}_\theta + \frac{2Eh}{R\pi}\left[A_{1,0}(t) + \frac{A_{3,0}(t)}{3} + \frac{A_{5,0}(t)}{5}\right]\right\} - \bar{N}_{x\theta}xR\theta, \quad (36)$$

where $\bar{N}_x$, $\bar{N}_\theta$ and $\bar{N}_{x\theta}$ are the in-plane restraint stresses generated at the ends of the shell, as a consequence of the in-plane constraints on average. Equation (36) is not the most general homogeneous solution, but it is chosen in order to satisfy the boundary conditions on average. In fact, it satisfies equations (3) on average as a consequence of (i) the contribution of F_p to $\bar{N}_\theta$ being $(2\pi RL)^{-1}\int_0^L\int_0^{2\pi}[\partial^2 F_p/\partial x^2]R\,\mathrm{d}\theta\,\mathrm{d}x$ and (ii) contributions of F_p to $\bar{N}_x$ and $\bar{N}_{x\theta}$ being zero. Boundary conditions (34, 35) allow one to express the in-plane restraint stresses $\bar{N}_x$, $\bar{N}_\theta$ and $\bar{N}_{x\theta}$, see equations (4–6), in terms of w and its derivatives. For case 1 they give

$$\bar{N}_x = 0, \quad (37a)$$

$$(1-\nu^2)\frac{\bar{N}_\theta}{Eh} = \frac{1}{2\pi RL}\int_0^{2\pi}\int_0^L\left[(\nu^2-1)\frac{w}{R} + \frac{1-\nu^2}{2}\left(\frac{\partial w}{R\partial\theta}\right)^2\right]\mathrm{d}xR\,\mathrm{d}\theta, \quad (38a)$$

$$\bar{N}_{x\theta} = 0; \quad (39a)$$

while for case 2, they give

$$(1-\nu^2)\frac{\bar{N}_x}{Eh} = \frac{1}{2\pi RL}\int_0^{2\pi}\int_0^L\left[-\frac{\nu w}{R} + \frac{1}{2}\left(\frac{\partial w}{\partial x}\right)^2 + \frac{\nu}{2}\left(\frac{\partial w}{R\partial\theta}\right)^2\right]\mathrm{d}xR\,\mathrm{d}\theta, \quad (37b)$$

$$(1-\nu^2)\frac{\bar{N}_\theta}{Eh} = \frac{1}{2\pi RL}\int_0^{2\pi}\int_0^L\left[-\frac{w}{R} + \frac{\nu}{2}\left(\frac{\partial w}{\partial x}\right)^2 + \frac{1}{2}\left(\frac{\partial w}{R\partial\theta}\right)^2\right]\mathrm{d}xR\,\mathrm{d}\theta, \quad (38b)$$

$$\bar{N}_{x\theta} = 0. \quad (39b)$$

For case 1, simple calculations give

$$\bar{N}_\theta = Eh\left\{-\frac{2}{\pi R}\left[A_{1,0}(t) + \frac{A_{3,0}(t)}{3} + \frac{A_{5,0}(t)}{5}\right] + \frac{n^2}{8R^2}[A_{1,n}^2(t) + B_{1,n}^2(t) + A_{2,n}^2(t) + B_{2,n}^2(t)]\right\}; \quad (40)$$

for case 2, the results are

$$\bar{N}_x = \frac{Eh}{1-\nu^2}\left\{\frac{-2\nu}{\pi R}\left[A_{1,0}(t) + \frac{A_{3,0}(t)}{3} + \frac{A_{5,0}(t)}{5}\right] + \frac{\pi^2}{4L^2}[A_{1,0}^2(t) + 9A_{3,0}^2(t) + 25A_{5,0}^2(t)]\right.$$

$$\left. + \frac{1}{8}\left(\frac{\pi^2}{L^2} + \frac{\nu n^2}{R^2}\right)[A_{1,n}^2(t) + B_{1,n}^2(t)] + \frac{1}{2}\left(\frac{\pi^2}{L^2} + \frac{\nu n^2}{4R^2}\right)[A_{2,n}^2(t) + B_{2,n}^2(t)]\right\}, \quad (41)$$

$$\bar{N}_\theta = \frac{Eh}{1-\nu^2}\left\{\frac{-2}{\pi R}\left[A_{1,0}(t) + \frac{A_{3,0}(t)}{3} + \frac{A_{5,0}(t)}{5}\right] + \frac{\nu\pi^2}{4L^2}[A_{1,0}^2(t) + 9A_{3,0}^2(t) + 25A_{5,0}^2(t)]\right.$$

$$\left. + \frac{1}{8}\left(\frac{\nu\pi^2}{L^2} + \frac{n^2}{R^2}\right)[A_{1,n}^2(t) + B_{1,n}^2(t)] + \frac{1}{2}\left(\frac{\nu\pi^2}{L^2} + \frac{n^2}{4R^2}\right)[A_{2,n}^2(t) + B_{2,n}^2(t)]\right\}. \quad (42)$$

At this point, all the terms involved in the equation of motion, equation (1), have been evaluated.

By using the Galerkin method, generally seven second-order ordinary, coupled non-linear differential equations are obtained for the variables $A_{1,n}(t)$, $B_{1,n}(t)$, $A_{2,n}(t)$, $B_{2,n}(t)$, $A_{1,0}(t)$, $A_{3,0}(t)$ and $A_{5,0}(t)$, by successively weighting the single original equation with suitable functions z_s, $s = 1, \ldots, 7$, and integrating over the shell middle surface. The weighting functions z_s are defined as

$$z_s(x, \theta) = \left\{\begin{array}{ll} \cos(n\theta)\sin(\pi x/L) & \text{for } s = 1 \\ \sin(n\theta)\sin(\pi x/L) & \text{for } s = 2 \\ \cos(n\theta)\sin(2\pi x/L) & \text{for } s = 3 \\ \sin(n\theta)\sin(2\pi x/L) & \text{for } s = 4 \\ \sin(\pi x/L) & \text{for } s = 5 \\ \sin(3\pi x/L) & \text{for } s = 6 \\ \sin(5\pi x/L) & \text{for } s = 7 \end{array}\right\}. \quad (43)$$

The Galerkin projection of the equation of motion (1), in this case, may be expressed as

$$\langle[\text{equation (1)}], z_s\rangle = \int_0^{2\pi}\int_0^L [\text{equation (1)}]\, z_s(x, \theta)\, \mathrm{d}x\, \mathrm{d}\theta, \quad (44)$$

and it has been performed by using the *Mathematica* computer software [29].

4.1. EQUATIONS OF MOTION FOR THE WEAVER AND UNNY MODEL

The Galerkin projections in the case of a shell with internal flow modelled by the Weaver and Unny theory and subjected to an external excitation $f = f_n \cos(n\theta)\sin(\pi x/L)\cos(\omega t)$ of unspecified physical origin, give the following system of four equations.

The first one is

$$\ddot{A}_{1,n}(t)+2\zeta_{1,n}\omega_{1,n}\dot{A}_{1,n}(t)+\left(\omega_{1,n}^2-\frac{U^2\rho_F L^2\pi^2\xi_{0,n}}{m_1}\right)A_{1,n}(t)-\frac{4U\rho_F L^2\pi^2\lambda_{1,n}}{m_1}\dot{A}_{2,n}(t)$$

$$+h_1A_{1,n}^3(t)+h_1A_{1,n}(t)B_{1,n}^2(t)+h_2A_{1,n}(t)A_{2,n}^2(t)+h_3A_{1,n}(t)B_{2,n}^2(t)$$

$$+h_4A_{2,n}(t)B_{1,n}(t)B_{2,n}(t)=\frac{\pi L}{2m_1}f_n\cos(\omega t), \tag{45a}$$

where

$$\xi_{i,n}=\int_{-\infty}^{\infty}\frac{\mathrm{I}_n(\alpha R)}{\mathrm{I}_n'(\alpha R)}\frac{1+\cos(\alpha L)}{(\pi^2-\alpha^2L^2)^2}\alpha^{1-i}\,\mathrm{d}\alpha \quad \text{for } i=0,\,2,$$

$$m_1=\rho h\pi L/2+\rho_F L^2\pi^2\xi_{2,n},$$

$$\lambda_{i,n}=\int_{-\infty}^{\infty}\frac{\mathrm{I}_n(\alpha R)}{\mathrm{I}_n'(\alpha R)}\frac{\sin(\alpha L)}{(4\pi^2-\alpha^2L^2)(\pi^2-\alpha^2L^2)}\alpha^{1-i}\,\mathrm{d}\alpha \quad \text{for } i=0,\,1,\,2,$$

$$\omega_{1,n}^2=\frac{\pi L}{2}\left[D\left(\frac{\pi^2}{L^2}+\frac{n^2}{R^2}\right)^2+\frac{Eh\pi^4}{R^2L^4}\Big/\left(\frac{\pi^2}{L^2}+\frac{n^2}{R^2}\right)^2\right]\Big/m_1, \qquad \zeta_{1,n}=ch\frac{\pi L}{2}\Big/(2\omega_{1,n}m_1),$$

and h_i, $i=1,\ldots,4$, are coefficients depending on geometry, material properties and n that arise from projections of the part of equation (1) involving the stress function F.

The second equation of the system is

$$\ddot{B}_{1,n}(t)+2\zeta_{1,n}\omega_{1,n}\dot{B}_{1,n}(t)+\left(\omega_{1,n}^2-\frac{U^2\rho_F L^2\pi^2\xi_{0,n}}{m_1}\right)B_{1,n}(t)-\frac{4U\rho_F L^2\pi^2\lambda_{1,n}}{m_1}\dot{B}_{2,n}(t)$$

$$+h_1B_{1,n}^3(t)+h_1B_{1,n}(t)A_{1,n}^2(t)+h_2B_{1,n}(t)B_{2,n}^2(t)+h_3B_{1,n}(t)A_{2,n}^2(t)$$

$$+h_4B_{2,n}(t)A_{1,n}(t)A_{2,n}(t)=0. \tag{45b}$$

The third equation is

$$\ddot{A}_{2,n}(t)+2\zeta_{2,n}\omega_{2,n}\dot{A}_{2,n}(t)+\left(\omega_{2,n}^2-\frac{4U^2\rho_F L^2\pi^2\eta_{0,n}}{m_2}\right)A_{2n}(t)+\frac{8U\rho_F L^2\pi^2\lambda_{1,n}}{m_2}\dot{A}_{1,n}(t)$$

$$+k_1A_{2,n}^3(t)+k_1A_{2,n}(t)B_{2,n}^2(t)+k_2A_{2,n}(t)A_{1,n}^2(t)+k_3A_{2,n}(t)B_{1,n}^2(t)$$

$$+k_4A_{1,n}(t)B_{1,n}(t)B_{2,n}(t)=0, \tag{45c}$$

where

$$\eta_{i,n} = \int_{-\infty}^{\infty} \frac{\mathrm{I}_n(\alpha R)}{\mathrm{I}'_n(\alpha R)} \frac{1 - \cos(\alpha L)}{(4\pi^2 - \alpha^2 L^2)^2} \alpha^{1-i} \mathrm{d}\alpha \quad \text{for } i = 0, 2,$$

$$m_2 = \rho \mathrm{h} \pi L/2 + 4\rho_F L^2 \pi^2 \eta_{2,n},$$

$$\omega_{2,n}^2 = \frac{\pi L}{2} \left[D\left(\frac{4\pi^2}{L^2} + \frac{n^2}{R^2}\right)^2 + \frac{16Eh\pi^4}{R^2 L^4} \Big/ \left(\frac{4\pi^2}{L^2} + \frac{n^2}{R^2}\right)^2 \right] \Big/ m_2,$$

$$\zeta_{2,n} = ch \frac{\pi L}{2} \Big/ (2\omega_{2,n} m_2),$$

and k_i, $i = 1, \ldots, 4$, are appropriate coefficients.

The last equation of the system is

$$\ddot{B}_{2,n}(t) + 2\zeta_{2,n}\omega_{2,n}\dot{B}_{2,n}(t) + \left(\omega_{2,n}^2 - \frac{4U^2\rho_F L^2 \pi^2 \eta_{0,n}}{m_2}\right) B_{2,n}(t) + \frac{8U\rho_F L^2 \pi^2 \lambda_{1,n}}{m_2} \dot{B}_{1,n}(t)$$

$$+ k_1 B_{2,n}^3(t) + k_1 B_{2,n}(t) A_{2,n}^2(t) + k_2 B_{2,n}(t) B_{1,n}^2(t) + k_3 B_{2,n}(t) A_{1,n}^2(t)$$

$$+ k_4 B_{1,n}(t) A_{1,n}(t) A_{2,n}(t) = 0. \tag{45d}$$

System (45) has been obtained for boundary condition $N_x = 0$ (case 1); for condition $u = 0$ some additional non-linear terms appear in the equations.

As a consequence of the assumed external or flow-related excitation appearing only in equation (45a), it is possible to have a solution for $B_{1,n}(t) = 0$ and $B_{2,n}(t) = 0$ [for $A_{1,n}(t) \neq 0$, $A_{2,n}(t) \neq 0$]; this solution gives the so-called *driven mode*. The solution for $B_{1,n}(t) \neq 0$ and $B_{2,n}(t) \neq 0$ gives both the driven mode, related to $A_{1,}(t)$ and $A_{2,n}(t)$, and the *companion mode*, related to $B_{1,n}(t)$ and $B_{2,n}(t)$.

4.2. EQUATIONS OF MOTION FOR THE PAÏDOUSSIS AND DENISE MODEL

The Galerkin projections in the case of a shell with flowing fluid inside modelled by the Païdoussis and Denise's theory and subjected to an external excitation, give the following system of seven equations. The first one is

$$\ddot{A}_{1,n}(t) + 2\zeta_{1,n}\omega_{1,n}\dot{A}_{1,n}(t) + \left(\omega_{1,n}^2 - \frac{U^2\rho_F \pi^2 \mathrm{I}_n(\pi R/L)}{2m_1 \mathrm{I}'_n(\pi R/L)}\right) A_{1,n}(t)$$

$$- \frac{4U\rho_F L \mathrm{I}_n(2\pi R/L)}{3m_1 \mathrm{I}'_n(2\pi R/L)} \dot{A}_{2,n}(t)$$

$$+ h_1 A_{1,n}^3(t) + h_1\, A_{1,n}(t) B_{1,n}^2(t) + h_2\, A_{1,n}(t) A_{2,n}^2(t) + h_3\, A_{1,n}(t) B_{2,n}^2(t)$$

$$+ h_4\, A_{2,n}(t) B_{1,n}(t) B_{2,n}(t) + h_5\, A_{1,n}(t) A_{1,0}(t) + h_6\, A_{1,n}(t) A_{3,0}(t)$$

$$+ h_7\, A_{1,n}(t) A_{5,0}(t) + h_8\, A_{1,n}(t) A_{1,0}^2(t) + h_9\, A_{1,n}(t) A_{3,0}^2(t) + h_{10}\, A_{1,n}(t) A_{5,0}^2(t)$$

$$+ h_{11}\, A_{1,n}(t) A_{1,0}(t) A_{3,0}(t) + h_{12}\, A_{1,n}(t) A_{3,0}(t) A_{5,0}(t) = \frac{\pi L}{2m_1} f_n \cos(\omega t), \tag{46a}$$

where

$$m_1 = \rho h \pi L/2 + \rho_F L^2 \mathrm{I}_n(\pi R/L)/[2\mathrm{I}_n'(\pi R/L)],$$

$$\omega_{1,n}^2 = \frac{\pi L}{2}\left[D\left(\frac{\pi^2}{L^2} + \frac{n^2}{R^2}\right)^2 + \frac{Eh\pi^4}{R^2 L^4}\Big/\left(\frac{\pi^2}{L^2} + \frac{n^2}{R^2}\right)^2 \right]\Big/ m_1,$$

$$\zeta_{1,n} = ch\frac{\pi L}{2}\Big/(2\omega_{1,n} m_1),$$

and h_i, $i = 1, \ldots, 12$, are coefficients depending on geometry, material properties and n that arise from projections of the part of equation (1) involving the stress function F.

The second equation is

$$\ddot{B}_{1,n}(t) + 2\zeta_{1,n}\omega_{1,n}\dot{B}_{1,n}(t) + \left(\omega_{1,n}^2 - \frac{U^2\rho_F\pi^2 \mathrm{I}_n(\pi R/L)}{2m_1 \mathrm{I}_n'(\pi R/L)}\right) B_{1,n}(t) - \frac{4U\rho_F L \mathrm{I}_n(2\pi R/L)}{3m_1 \mathrm{I}_n'(2\pi R/L)}\dot{B}_{2,n}(t)$$

$$+ h_1 B_{1,n}^3(t) + h_1\, B_{1,n}(t) A_{1,n}^2(t) + h_2\, B_{1,n}(t) B_{2,n}^2(t) + h_3\, B_{1,n}(t) A_{2,n}^2(t)$$

$$+ h_4\, B_{2,n}(t) A_{1,n}(t) A_{2,n}(t) + h_5\, B_{1,n}(t) A_{1,0}(t) + h_6\, B_{1,n}(t) A_{3,0}(t)$$

$$+ h_7\, B_{1,n}(t) A_{5,0}(t) + h_8\, B_{1,n}(t) A_{1,0}^2(t) + h_9\, B_{1,n}(t) A_{3,0}^2(t) + h_{10}\, B_{1,n}(t) A_{5,0}^2(t)$$

$$+ h_{11}\, B_{1,n}(t) A_{1,0}(t) A_{3,0}(t) + h_{12}\, B_{1,n}(t) A_{3,0}(t) A_{5,0}(t) = 0. \tag{46b}$$

The third equation is

$$\ddot{A}_{2,n}(t) + 2\zeta_{2,n}\omega_{2,n}\dot{A}_{2,n}(t) + \left(\omega_{2,n}^2 - \frac{U^2\rho_F\pi^2 \mathrm{I}_n(2\pi R/L)}{m_2 \mathrm{I}_n'(2\pi R/L)}\right) A_{2,n}(t) + \frac{8U\rho_F L \mathrm{I}_n(\pi R/L)}{3m_2 \mathrm{I}_n'(\pi R/L)}\dot{A}_{1,n}(t)$$

$$+ k_1 A_{2,n}^3(t) + k_1\, A_{2,n}(t) B_{2,n}^2(t) + k_2\, A_{2,n}(t) A_{1,n}^2(t) + k_3\, A_{2,n}(t) B_{1,n}^2(t)$$

$$+ k_4 A_{1,n}(t) B_{1,n}(t) B_{2,n}(t) + k_5 A_{2,n}(t) A_{1,0}(t) + k_6 A_{2,n}(t) A_{3,0}(t)$$

$$+ k_7\, A_{2,n}(t) A_{5,0}(t) + k_8\, A_{2,n}(t) A_{1,0}^2(t) + k_9\, A_{2,n}(t) A_{3,0}^2(t) + k_{10}\, A_{2,n}(t) A_{5,0}^2(t)$$

$$+ k_{11}\, A_{2,n}(t) A_{1,0}(t) A_{3,0}(t) + k_{12}\, A_{2,n}(t) A_{1,0}(t) A_{5,0}(t) = 0, \tag{46c}$$

where

$$m_2 = \rho h\pi L/2 + \rho_F L^2 \mathrm{I}_n(2\pi R/L)/[4\mathrm{I}'_n(2\pi R/L)],$$

$$\omega_{2,n}^2 = \frac{\pi L}{2}\left[D\left(\frac{4\pi^2}{L^2}+\frac{n^2}{R^2}\right)^2 + \frac{16Eh\pi^4}{R^2L^4}\Big/\left(\frac{4\pi^2}{L^2}+\frac{n^2}{R^2}\right)^2\right]\Big/ m_2$$

$$\zeta_{2,n} = ch\,\frac{\pi L}{2}\Big/(2\omega_{2,n}m_2),$$

and k_i, $i = 1, \ldots, 12$, are appropriate coefficients.

The fourth equation is

$$\ddot{B}_{2,n}(t)+2\zeta_{2,n}\omega_{2,n}\dot{B}_{2,n}(t)+\left(\omega_{2,n}^2-\frac{U^2\rho_F\pi^2\mathrm{I}_n(2\pi R/L)}{m_2\mathrm{I}'_n(2\pi R/L)}\right)B_{2,n}(t)+\frac{8U\rho_F L\mathrm{I}_n(\pi R/L)}{3m_2\mathrm{I}'_n(\pi R/L)}\dot{B}_{1,n}(t)$$

$$+ k_1 B_{2,n}^3(t) + k_1 B_{2,n}(t)A_{2,n}^2(t) + k_2 B_{2,n}(t)B_{1,n}^2(t) + k_3 B_{2,n}(t)A_{1,n}^2(t)$$

$$+ k_4 B_{1,n}(t)A_{1,n}(t)A_{2,n}(t) + k_5 B_{2,n}(t)A_{1,0}(t) + k_6 B_{2,n}(t)A_{3,0}(t)$$

$$+ k_7 B_{2,n}(t)A_{5,0}(t) + k_8 B_{2,n}(t)A_{1,0}^2(t) + k_9 B_{2,n}(t)A_{3,0}^2(t) + k_{10} B_{2,n}(t)A_{5,0}^2(t)$$

$$+ k_{11} B_{2,n}(t)A_{1,0}(t)A_{3,0}(t) + k_{12} B_{2,n}(t)A_{1,0}(t)A_{5,0}(t) = 0. \tag{46d}$$

The fifth equation, that is related to the first axisymmetric degree of freedom, is

$$\ddot{A}_{1,0}(t) + 2\zeta_{1,0}\omega_{1,0}\dot{A}_{1,0}(t) + \left(\omega_{1,0}^2 - \frac{U^2\rho_F\pi^2\mathrm{I}_0(\pi R/L)}{m_{1,0}\mathrm{I}'_0(\pi R/L)}\right)A_{1,0}(t) + l_1 A_{1,0}(t)A_{1,n}^2(t)$$

$$+ l_1 A_{1,0}(t)B_{1,n}^2(t) + l_2 A_{1,0}(t)A_{2,n}^2(t) + l_2 A_{1,0}(t)B_{2,n}^2(t) + l_3 A_{1,n}^2(t) + l_3 B_{1,n}^2(t)$$

$$+ l_4 A_{2,n}^2(t) + l_4 B_{2,n}^2(t) + l_5 A_{3,0}(t)A_{1,n}^2(t) + l_5 A_{3,0}(t)B_{1,n}^2(t) + l_6 A_{3,0}(t)A_{2,n}^2(t)$$

$$+ l_6 A_{3,0}(t)B_{2,n}^2(t) + l_7 A_{5,0}(t)A_{2,n}^2(t) + l_7 A_{5,0}(t)B_{2,n}^2(t) = 0, \tag{46e}$$

where

$$m_{1,0} = \rho h\pi L + \rho_F L^2 \mathrm{I}_0(\pi R/L)/\mathrm{I}'_0(\pi R/L),$$

$$\omega_{1,0}^2 = \frac{\pi L}{m_{1,0}}\left(\frac{D\pi^4}{L^4}+\frac{Eh}{R^2}\right), \quad \zeta_{1,0} = ch\pi L/(2\omega_{1,0}m_{1,0}),$$

and l_i, $i = 1, \ldots, 7$, are appropriate coefficients.

The sixth equation is

$$\ddot{A}_{3,0}(t) + 2\zeta_{3,0}\omega_{3,0}\dot{A}_{3,0}(t) + \left(\omega_{3,0}^2 - \frac{3U^2\rho_F\pi^2 \mathrm{I}_0(3\pi R/L)}{m_{3,0}\mathrm{I}_0'(3\pi R/L)}\right)A_{3,0}(t) + n_1 A_{3,0}(t)A_{1,n}^2(t)$$

$$+ n_1 A_{3,0}(t)B_{1,n}^2(t) + n_2 A_{3,0}(t)A_{2n}^2(t) + n_2 A_{3,0}(t)B_{2,n}^2(t) + n_3 A_{1,n}^2(t) + n_3 B_{1,n}^2(t)$$

$$+ n_4 A_{2,n}^2(t) + n_4 B_{2,n}^2(t) + n_5 A_{1,0}(t)A_{1,n}^2(t) + n_5 A_{1,0}(t)B_{1,n}^2(t) + n_6 A_{1,0}(t)A_{2,n}^2(t)$$

$$+ n_6 A_{1,0}(t)B_{2,n}^2(t) + n_7 A_{5,0}(t)A_{1,n}^2(t) + n_7 A_{5,0}(t)B_{1,n}^2(t) = 0, \tag{46f}$$

where

$$m_{3,0} = \rho h\pi L + \rho_F L^2 \mathrm{I}_0(3\pi R/L)/[3\mathrm{I}_0'(3\pi R/L)],$$

$$\omega_{3,0}^2 = \frac{\pi L}{m_{3,0}}\left(\frac{81D\pi^4}{L^4} + \frac{Eh}{R^2}\right), \qquad \zeta_{3,0} = ch\pi L/(2\omega_{3,0}m_{3,0}),$$

and n_i, $i = 1, \ldots, 7$, are appropriate coefficients.

The last equation is

$$\ddot{A}_{5,0}(t) + 2\zeta_{5,0}\omega_{5,0}\dot{A}_{5,0}(t) + \left(\omega_{5,0}^2 - \frac{5U^2\rho_F\pi^2 \mathrm{I}_0(5\pi R/L)}{m_{5,0}\mathrm{I}_0'(5\pi R/L)}\right)A_{5,0}(t) + p_1 A_{5,0}(t)A_{1,n}^2(t)$$

$$+ p_1 A_{5,0}(t)B_{1,n}^2(t) + p_2 A_{5,0}(t)A_{2,n}^2(t) + p_2 A_{5,0}(t)B_{2,n}^2(t) + p_3 A_{1,n}^2(t) + p_3 B_{1,n}^2(t)$$

$$+ p_4 A_{2,n}^2(t) + p_4 B_{2,n}^2(t) + p_5 A_{1,0}(t)A_{2,n}^2(t) + p_5 A_{1,0}(t)B_{2,n}^2(t) + p_6 A_{3,0}(t)A_{1,n}^2(t)$$

$$+ p_6 A_{3,0}(t)B_{1,n}^2(t) = 0, \tag{46g}$$

where

$$m_{5,0} = \rho h\pi L + \rho_F L^2 \mathrm{I}_0(5\pi R/L)/[5\mathrm{I}_0'(5\pi R/L)],$$

$$\omega_{5,0}^2 = \frac{\pi L}{m_{5,0}}\left(\frac{625D\pi^4}{L^4} + \frac{Eh}{R^2}\right), \quad \zeta_{5,0} = \frac{ch\pi L}{(2\omega_{5,0}m_{5,0})},$$

and p_i, $i = 1, \ldots, 6$, are appropriate coefficients.

System (46) was obtained for boundary condition $N_x = 0$ (case 1); for condition $u = 0$, some additional non-linear terms appear in the equations.

Equations (45) and (46) can be integrated by means of standard numerical schemes, such as a Runge–Kutta routine.

5. TRAVELLING-WAVE MODE

The presence of the companion mode in the periodic response of the shell leads to the appearance of travelling waves. The flexural mode shapes are represented by equation (7b). Upon supposing that $A_{1,n}(t) = \tilde{A}_{1,n}\cos(\omega t + \vartheta_1)$, $B_{1,n}(t) =$

$\tilde{B}_{1,n}\cos(\omega t + \vartheta_2)$, $A_{2,n}(t) = \tilde{A}_{2,n}\cos(\omega t + \vartheta_3)$ and $B_{2,n}(t) = \tilde{B}_{2,n}\cos(\omega t + \vartheta_4)$, equation (7b) can be rearranged as

$$w = \{[\tilde{A}_{1,n}\cos(\omega t + \vartheta_1) + \tilde{B}_{1,n}\sin(\omega t + \vartheta_2)]\cos(n\theta) + \tilde{B}_{1,n}\sin(n\theta - \omega t - \vartheta_2)\}\sin(\pi x/L)$$

$$+ \{[\tilde{A}_{2,n}\cos(\omega t + \vartheta_3) + \tilde{B}_{2,n}\sin(\omega t + \vartheta_4)]\cos(n\theta)$$

$$+ \tilde{B}_{2,n}\sin(n\theta - \omega t - \vartheta_4)\}\sin(2\pi x/L) + O(\varepsilon^2), \tag{47}$$

where ϑ_1, ϑ_2, ϑ_3, and ϑ_4 are the phase constants in the solution of equations (45) and (46), ω is the radian frequency of the shell response, and ε is a small quantity. $O(\varepsilon^2)$ denotes small terms of higher order in the response of the shell [in equation (47) only first-order asymmetric terms are considered]. Equation (47) gives two travelling waves of amplitude $\tilde{B}_{1,n}$ and $\tilde{B}_{2,n}$ and radian frequency $\omega_T = \omega/n$, and two standing waves of radian frequency ω. The resulting standing wave with $m = 1$ is given by the sum of two standing waves, one of amplitude $\tilde{A}_{1,n}$ and the second of amplitude $\tilde{B}_{1,n}$, having the same radian frequency ω and the same shape, but having a phase difference of $\vartheta_2 - \vartheta_1 - \pi/2$ (similarly for $m = 2$). When $\vartheta_2 - \vartheta_1 \simeq \pi/2$, the amplitude of the resulting standing wave is almost $\tilde{A}_{1,n} + \tilde{B}_{1,n}$. The amplitude and frequency of the travelling wave solutions are not affected by phase relationship between driven and companion modes.

In general, the existence of driven and companion modes leads to the appearance of a circumferentially travelling wave and a standing wave; this phenomenon is related to the axial-symmetry of the system. As a consequence of both these modes appearing for forced and fluid-excited non-linear vibrations, this phenomenon represents a fundamental difference *vis-à-vis* linear vibrations.

6. NUMERICAL RESULTS

Numerical results were obtained for a case already studied in the literature, in order to allow a comparison. The case analyzed here was studied analytically by Weaver and Unny [2] by means of linear theory and it relates to a circular cylindrical shell, simply supported at the ends ($N_x = 0$), containing flowing water and having the following characteristics: $L/R = 2$, $h/R = 0{\cdot}01$, $E = 206 \times 10^9$ Pa, $\rho = 7850$ kg/m^3, $\rho_F = 1000$ kg/m^3 and $\nu = 0{\cdot}3$. It is studied for the circumferential wavenumber $n = 5$, which is associated with the lowest flow velocity for instability in the linear case. A non-dimensional fluid velocity V is introduced for convenience, defined as by Weaver and Unny [2] by $V = U/\{(\pi^2/L)[D/(\rho h)]^{1/2}\}$, with D as in equation (1); similary, a non-dimensional, generally complex, frequency Ω is defined as $\Omega = \omega/\{(\pi^2/L^2)[D/(\rho h)]^{1/2}\}$, ω being the corresponding radian frequency. In this section, the external excitation f is assumed to be zero.

6.1. LINEAR CASES

Figure 1 shows the real and imaginary part of the eigenvalues of the linearized equations of motion, obtained from equations (45) and (46) after deleting the

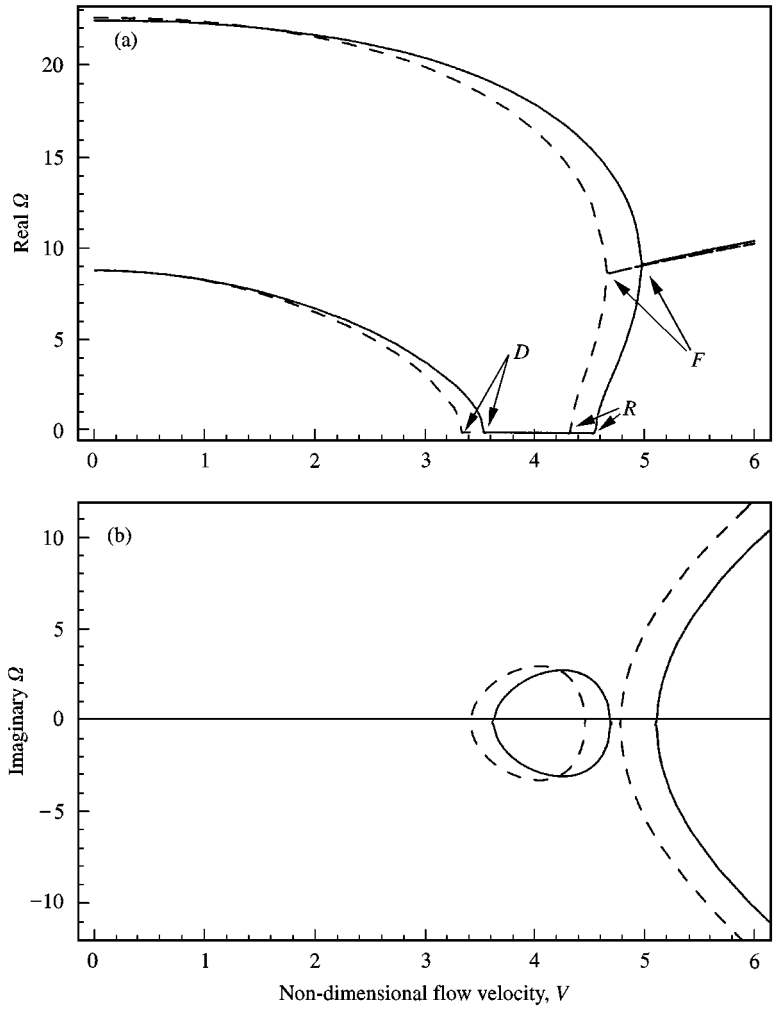

Figure 1. Non-dimensional complex frequency Ω obtained from the linearized equations without viscous damping ($\zeta = 0$) versus the non-dimensional flow velocity V: ——, model of Weaver and Unny; - - - -, model of Païdoussis and Denise; D divergence; R restabilization; F flutter. (a) Real part of Ω ; (b) imaginary part of Ω.

non-linear terms, for the fluid–structure interaction models of both Weaver and Unny and Païdoussis and Denise without dissipation ($\zeta = 0$). It is interesting to note that the two models give quite similar results in the linear range. Furthermore, the results obtained by using the Weaver and Unny model to describe the fluid–structure interaction are almost identical to those already published in reference [2]; it gives a validation of the linear part of the equations of motion. In Figure 1(a), the two curves give the real frequency Ω of the self-excited linearized system versus the non-dimensional fluid velocity V; the lower curve corresponds to the first longitudinal mode and the upper one to the second longitudinal mode. Figure 1(b) gives the imaginary component of the eigenfrequency, proportional to damping; when $\mathrm{Im}(\Omega) > 0$, the system is stable, while $\mathrm{Im}(\Omega) < 0$ means that the

system is unstable. Point D, where the first curve in Figure 1(a) reaches zero frequency, corresponds to static divergence of the system ($V = 3{\cdot}54$ or $3{\cdot}33$). The intersection of the second curve with the zero frequency gives the point of restabilization (R) of the system ($V = 4{\cdot}56$ or $4{\cdot}34$). Then, the merging of the first and second mode loci at point F corresponds to the onset of coupled-mode flutter ($V = 4{\cdot}97$ and $4{\cdot}65$). It should be emphasized here that, strictly, the existence of coupled-mode flutter cannot be decided by linear theory — cf. Holmes' work on the analogous thick-walled pipe problem, as discussed in references [11, 30], where it was shown by non-linear analysis that, in that case, coupled-mode flutter *cannot* occur. Obviously, in the linear case, no coupling with axisymmetric modes and with companion modes is present.

Figure 2 presents results for the Weaver and Unny model with viscous damping $\zeta = 0{\cdot}01$, which corresponds to a slightly overestimated damping with respect

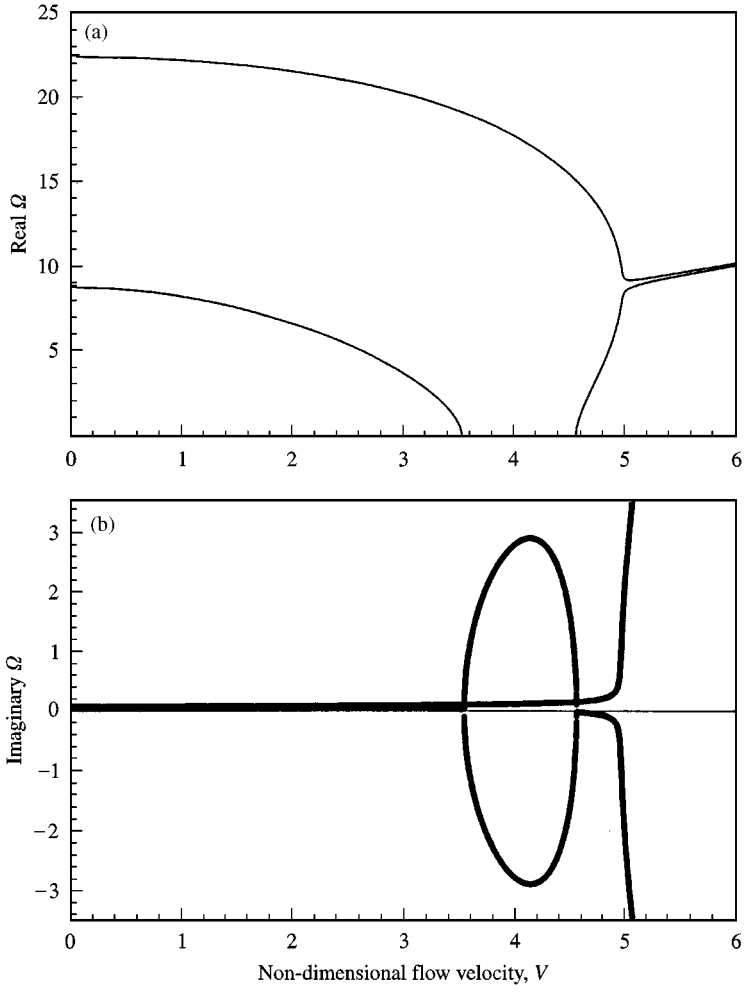

Figure 2. Non-dimensional complex frequency Ω obtained from the linearized equations with viscous damping $\zeta = 0{\cdot}01$ versus the non-dimensional flow velocity V for the Weaver and Unny model. (a) Real part of Ω; (b) imaginary part of Ω.

to some of the available experimental data for a shell containing water (see reference [31]). Two main differences can be observed with respect to the previous case: (i) one eigenfrequency with a small, positive imaginary part always exists, corresponding to damped vibrations due to the dissipation introduced; (ii) post-divergence restabilization of the system occurs no longer, since after the onset of divergence there is always an eigenvalue with a negative imaginary part. The intersections of the loci of Real(Ω) with the abscissa remain the same.

6.2. NON-LINEAR RESULTS WITHOUT COMPANION MODE PARTICIPATION

Simplified solutions can be obtained by eliminating from the equations of motion a few degrees of freedom. These solutions are of interest because they are strictly related to those obtained by solving the complete set of equations, as discussed in the following sections.

Solutions of equations (45) and (46) presented in this section have been obtained numerically by using the *Auto* software [32], based on a collocation method.

6.2.1. *Case with in-phase asymmetric modes*

In this case the condition $B_{1,n}(t) = B_{2,n}(t) = 0$, corresponding to the elimination of the companion mode, has been imposed over the whole time domain; consequently, the Weaver and Unny discretized model reduces to a two-degree-of-freedom system [equations (45)], while the Païdoussis and Denise model reduces to one of five degrees of freedom [equations (46)]. The two asymmetric modes retained are both associated with the same function $\cos(n\theta)$ in the angular direction, so they are "in-phase" or in "anti-phase" in θ.

The amplitudes of all of the generalized co-ordinates for the system including dissipation ($\zeta = 0{\cdot}01$) are shown in Figure 3 for the Weaver and Unny model and in Figure 4 for that of Païdoussis and Denise. In this latter case, in addition to the amplitudes of the first and second longitudinal modes, Figure 4(c–e) show the amplitude of the generalized co-ordinates associated with the axisymmetric deformation of the shell wall. All solutions found are non-oscillatory (stationary), i.e., they correspond to fixed points.

Figures 5 and 6 present the non-dimensional displacement of a point of the shell located at $x = L/4$ and circumferentially on an antinodal line versus the non-dimensional fluid velocity V for the models of Weaver and Unny and Païdoussis and Denise, respectively. Therefore, they have the same meaning as Figures 3 and 4, but the amplitude in this case is synthesized from the contributions of all the different degrees of freedom, so that it can be interpreted physically more easily.

One can first discuss the results obtained according to the Weaver and Unny model. It is seen in Figure 3(a) that this model predicts a divergence of hardening type at $V = 3{\cdot}54$, involving the first longitudinal mode (branch "1"). This bifurcated solution remains stable until $V = 5{\cdot}56$ is reached. However, at $V = 4{\cdot}56$ a second divergence arises (branch "2"), associated with the second longitudinal mode (Figure 3(b)); it becomes stable at $V = 4{\cdot}71$. Therefore, for $4.71 < V < 5{\cdot}56$, there

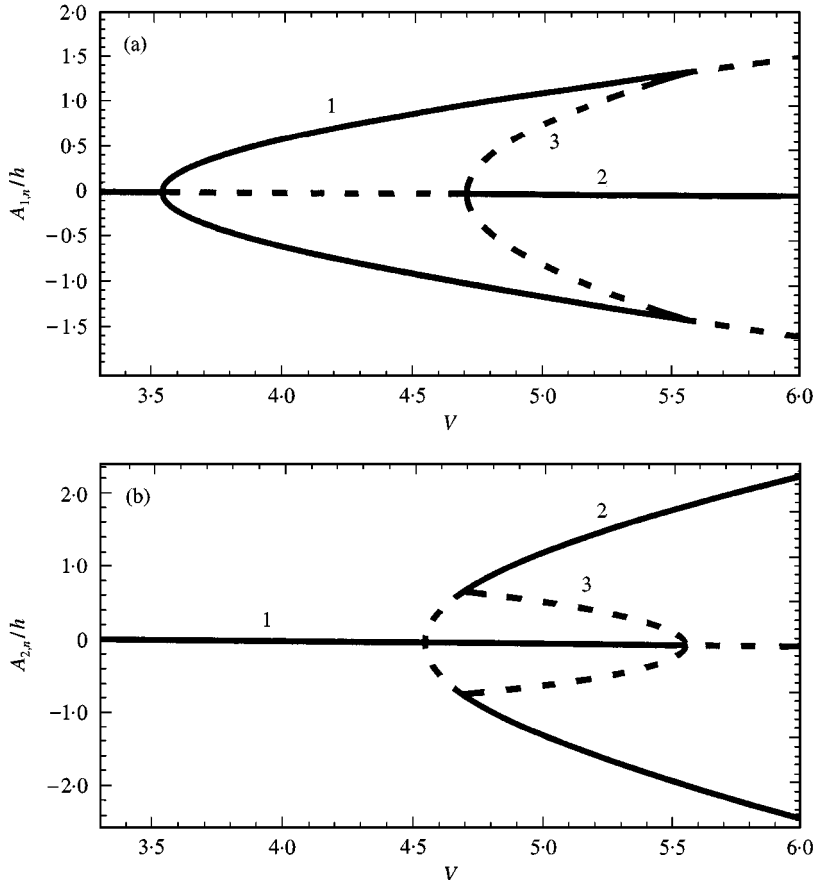

Figure 3. Amplitude of non-oscillatory (beyond divergence) solutions versus the non-dimensional flow velocity V; fluid model of Weaver and Unny, for in-phase modes and viscous damping $\zeta = 0{\cdot}01$. ——, Stable branches; - - - -, unstable branches. (a) Amplitude of the first longitudinal mode $A_{1,n}/h$; (b) amplitude of the second longitudinal mode $A_{2,n}/h$.

exist two stable solutions. Both symmetric branches for positive (inwards) and negative (outwards) shell displacement are stable, so that, in case of perturbation of the system, the solution can jump from one branch to the other. Indeed, for $4{\cdot}71 < V < 5{\cdot}56$ there exist four stable solutions and several unstable ones, as seen in Figure 5, and hence jumps should occur relatively "easily".

One can next consider the dynamics according to the Païdoussis and Denise model, which predicts an even more complex dynamical behaviour. Before discussing the dynamical behaviour *per se*, let us discuss the axisymmetric deformation of the shell, as shown in Figures 4(c–e). In particular, Figure 4(c) shows that the displacement related to the first axisymmetric mode is always positive, so that effectively it gives a contraction to the shell. Figure 4(d) shows that the third axisymmetric mode slightly reduces the contraction (away from the middle of the shell) given by the first axisymmetric mode for divergence in the first mode, but increases contraction for divergence in the second mode. The fifth axisymmetric

mode slightly reduces the contraction given by the other two axisymmetric modes; in fact, it is always negative, as shown in Figure 4(e).

One can now consider the dynamics, as shown in Figures 4 and 6 together. The system in this case loses stability in its first longitudinal mode by divergence (branch "1"), as seen in Figure 4(a), at $V = 3{\cdot}33$. However, in this case the bifurcation is strongly subcritical, which agrees with observations [1]; indeed, the range of V over which the system may diverge, given enough disturbance, extends over $1{\cdot}31 < V < 3{\cdot}33$! At $V = 1{\cdot}91$ there appears a second stable solution (divergence) associated with the second longitudinal mode (branch "2"). After this value of V, the system could easily undergo jumps, as a consequence of the coexistence of four stable solutions and some unstable solutions. Figure 6 shows that the system is no longer symmetrical with respect to zero displacement, as a consequence of the axisymmetric displacement. It is clear that inward axisymmetric displacements (positive) are larger than outwards displacements, as

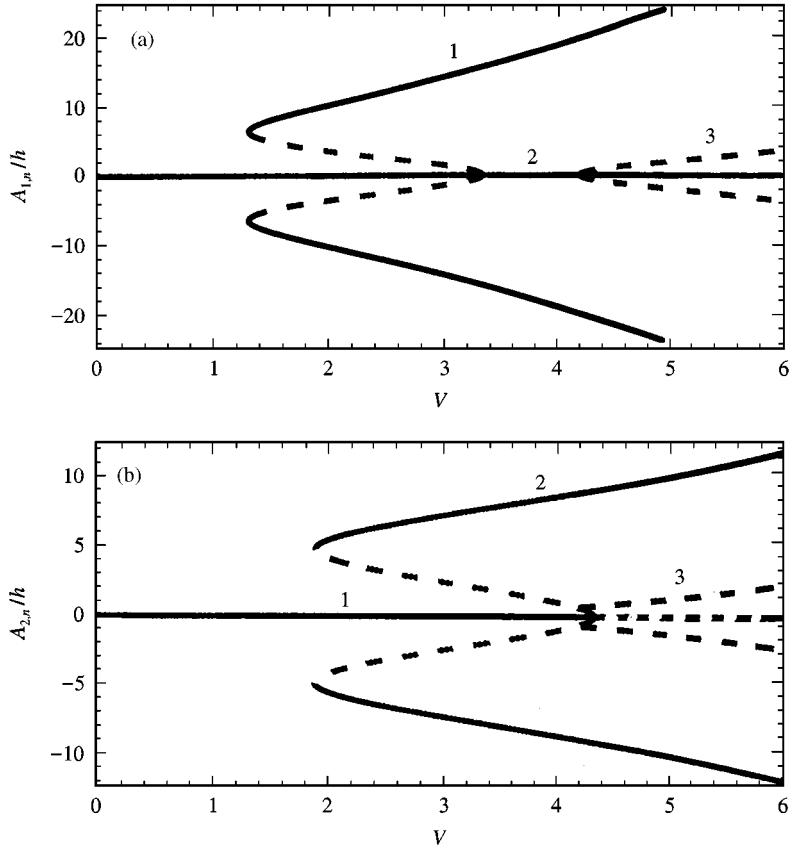

Figure 4. Amplitude of non-oscillatory solutions versus the non-dimensional flow velocity V; fluid model of Païdoussis and Denise, for in-phase modes and viscous damping $\zeta = 0{\cdot}01$. ——, Stable branches; - - - -, unstable branches. (a) Amplitude of the first longitudinal mode $A_{1,n}/h$; (b) amplitude of the second longitudinal mode $A_{2,n}/h$; (c) amplitude of the first axisymmetric mode $A_{1,0}/h$; (d) amplitude of the third axisymmetric mode $A_{3,0}/h$; (e) amplitude of the fifth axisymmetric mode $A_{5,0}/h$.

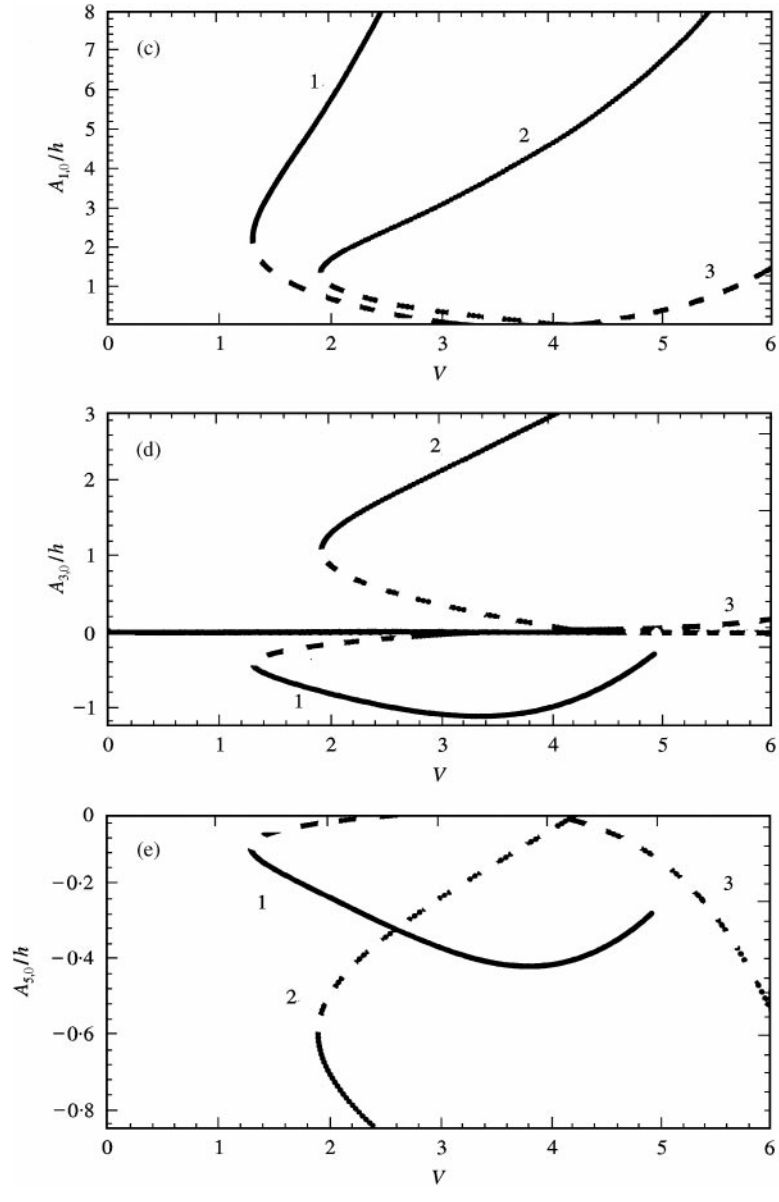

Figure 4. Continued.

already observed by others for non-linear shell vibrations; see, e.g., reference [18]. It is necessary to note that, for large inward displacement, the cross-section of the shell is diminished, so that the flow is impeded; this effect is not taken into account in the present linear model of interaction between fluid and shell.

It is very interesting to observe that the models of Weaver and Unny and Païdoussis and Denise give different kinds of non-linear dynamical behaviour of the system. In fact, this is closely related to the fact that the Weaver and Unny model does not allow for axisymmetric contraction of the shell, which

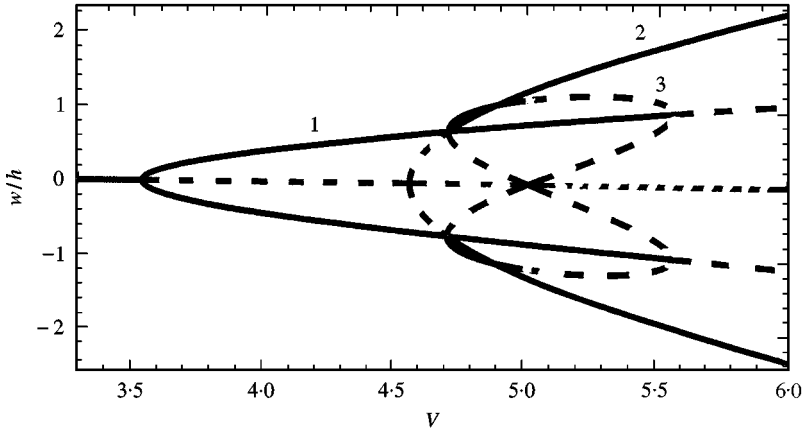

Figure 5. Non-oscillatory, non-dimensional displacement of a point on the shell located at $x = L/4$ (and circumferentially on an antinodal line) versus the non-dimensional flow velocity V; fluid model of Weaver and Unny with viscous damping $\zeta = 0{\cdot}01$. ——, Stable branches; - - - -, unstable branches.

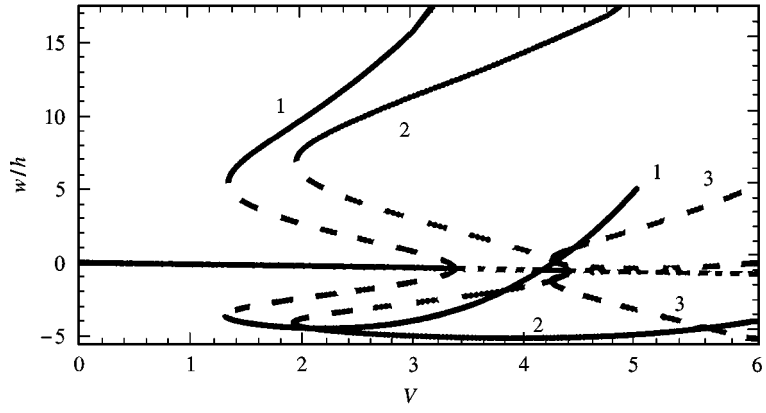

Figure 6. Non-oscillatory, non-dimensional displacement of a point on the shell located at $x = L/4$ (and circumferentially on an antinodal line) versus the non-dimensional flow velocity V; fluid model of Païdoussis and Denise with viscous damping $\zeta = 0{\cdot}01$. ——, Stable branches; - - - -, unstable branches.

is responsible for its softening behaviour [18]; consequently, the predicted system behaviour is of the hardening type after divergence. However, perfectly rigid extensions beyond the shell of infinite length are only a theoretical artifice for solving the mixed boundary value problem. Axisymmetric contraction is usually possible in engineering applications of shells, so that the behaviour obtained by using the model of Païdoussis and Denise must, in this respect, be considered closer to reality.

6.2.2. *Case with asymmetric modes orthogonal in* θ

In this case, the condition $B_{1,n}(t) = A_{2,n}(t) = 0$ has been imposed over the whole time domain, corresponding to consideration of two longitudinal modes involving two orthogonal functions in θ [modes rotated by $\pi/(2n)$]. Similarly to the previous

section, the Weaver and Unny discretized model reduces to a two-degree-of-freedom system [equation (45)], while the Païdoussis and Denise model reduces to one of five degrees of freedom [equation (46)].

The amplitudes of all of the generalized co-ordinates for the system including dissipation ($\zeta = 0{\cdot}01$) are shown in Figure 7 for the Weaver and Unny model and in Figure 8 for that of Païdoussis and Denise.

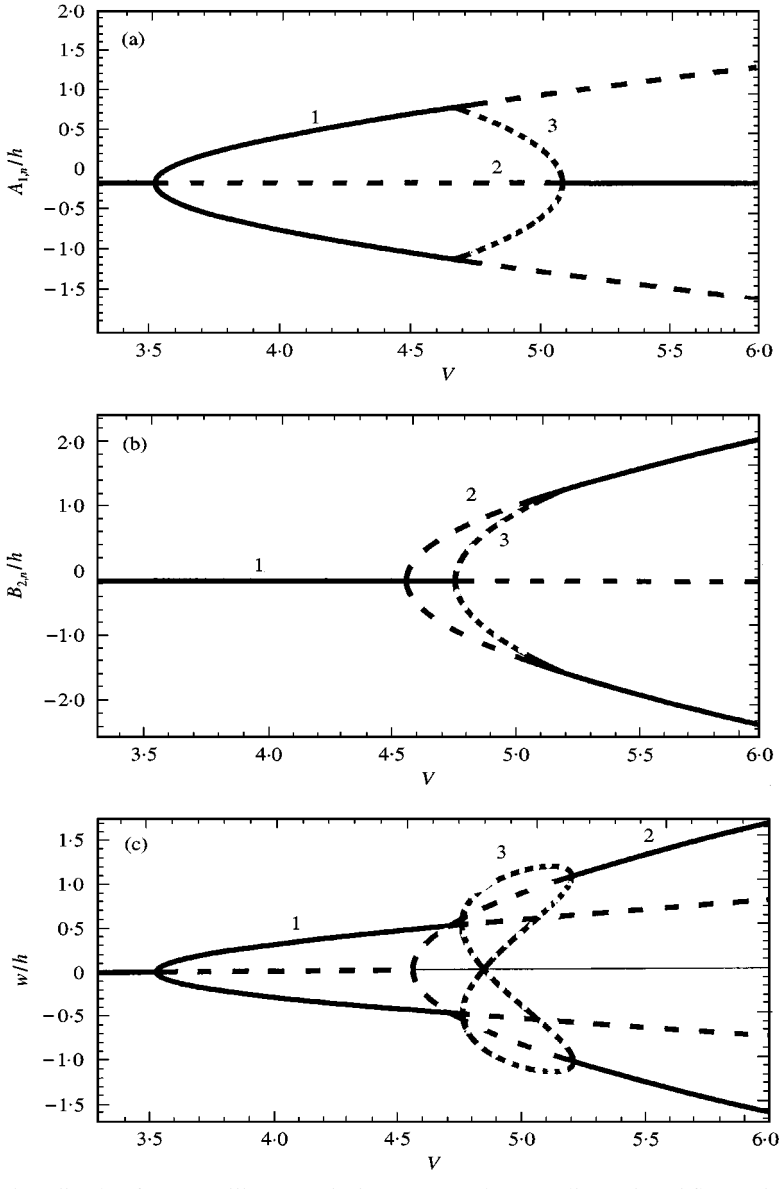

Figure 7. Amplitude of non-oscillatory solutions versus the non-dimensional flow velocity V; fluid model of Weaver and Unny, orthogonal modes and viscous damping $\zeta = 0{\cdot}01$. ——, Stable branches; - - - -, unstable branches. (a) Amplitude of the first longitudinal mode $A_{1,n}/h$; (b) amplitude of the second longitudinal mode $A_{2,n}/h$; (c) non-dimensional displacement of a point on the shell located at $x = L/4$ and circumferentially where $\sin(n\theta) = \cos(n\theta)$.

The results according to the Weaver and Unny model are considered first. Figure 7 shows that a different branch "3" appears with respect to the one detected in Figures 3 and 5. This is obtained with both of the retained degrees of freedom being active. In particular, the new detected coupled-mode solution is unstable (but it becomes stable when all the four degrees of freedom become active, as shown in section 6.4) and exists for $4{\cdot}76 < V < 5{\cdot}19$. Other interesting differences are that the divergence in the first mode (branch "1") is no longer stable for $V > 4{\cdot}76$, and divergence in the second mode (branch "2") is unstable for $V < 5{\cdot}19$.

Figure 8 relates to the results obtained via the Païdoussis and Denise model. In this case also, the coupled-mode solutions are different, compared to those presented in Figures 4 and 6. In particular, branch "3" is unstable, but becomes stable after the folding, i.e., for $V > 1{\cdot}84$, when all the seven degrees of freedom are

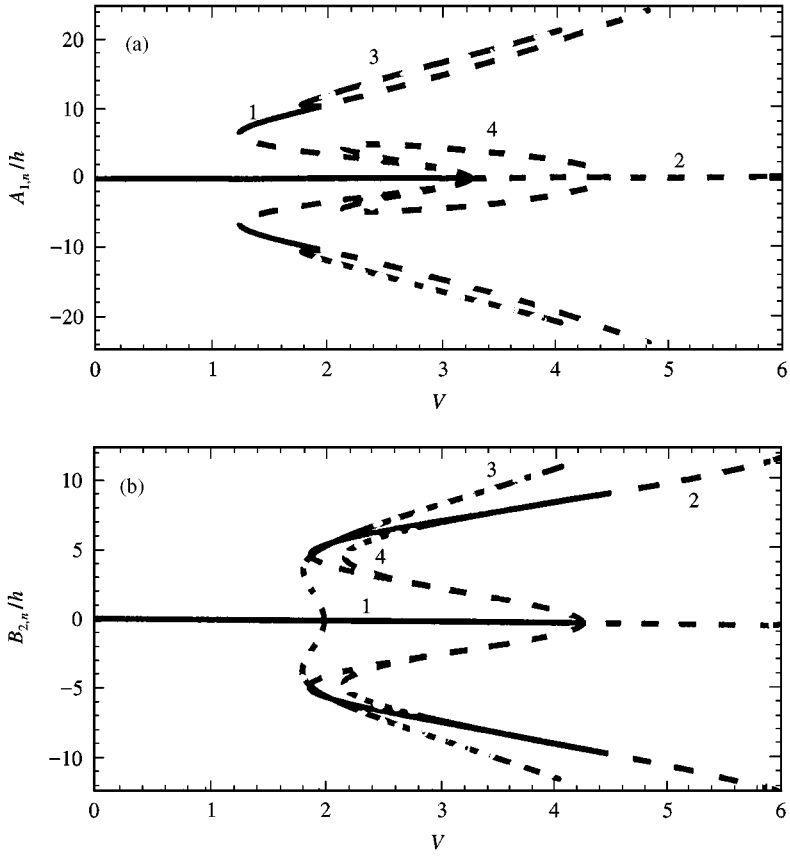

Figure 8. Amplitude of non-oscillatory solutions versus the non-dimensional flow velocity V; fluid model of Païdoussis and Denise, orthogonal modes and viscous damping $\zeta = 0{\cdot}01$. ——, Stable branches; - - - -, unstable branches. (a) Amplitude of the first longitudinal mode $A_{1,n}/h$; (b) amplitude of the second longitudinal mode $A_{2,n}/h$; (c) amplitude of the first axisymmetric mode $A_{1,0}/h$; (d) amplitude of the third axisymmetric mode $A_{3,0}/h$; (e) amplitude of the fifth axisymmetric mode $A_{5,0}/h$.

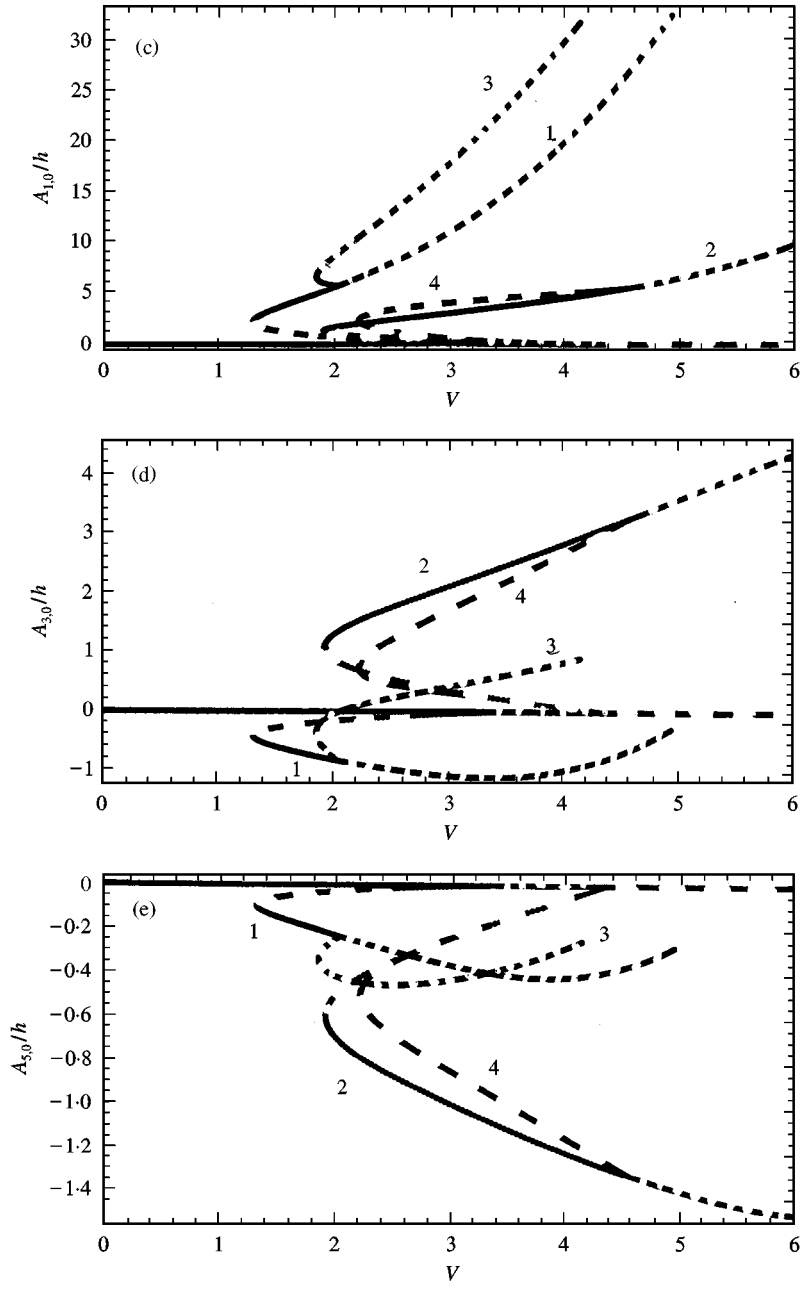

Figure 8. Continued.

active (see Section 6.4). As a consequence of divergence in both the first (branch "1") and second (branch "2") mode losing stability at $V = 2{\cdot}03$ and $V = 4{\cdot}56$, respectively, the only stable solution (when all the seven generalized co-ordinates are different from zero) at high flow velocity is the coupled-mode one.

6.3. ANALYTICAL EQUILIBRIUM POSITIONS

The stationary solutions are obtained by equations (45) and (46) by cancelling all the time-dependent terms; this gives algebraic equations that, in general, can be solved numerically. The case without companion-mode participation for the model of Weaver and Unny is particularly simple and analytical solutions can be given. Let us consider firstly the case with $B_{1,n} = B_{2,n} = 0$. In particular, the divergence amplitudes in the first longitudinal mode, i.e. the post-divergence fixed points, are given by

$$A_{1,n} = \pm\sqrt{(\alpha_1 U^2 - \omega_{1,n}^2)/h_1}, \quad A_{2,n} = 0, \tag{48}$$

and those in the second longitudinal mode by

$$A_{1,n} = 0, \quad A_{2,n} = \pm\sqrt{(\alpha_2 U^2 - \omega_{2,n}^2)/k_1}, \tag{49}$$

where $\alpha_1 = \rho_F L^2\pi^2\xi_{0,n}/m_1$, $\alpha_2 = 4\rho_F L^2\pi^2\eta_{0,n}/m_2$ and the other symbols are defined in section 4. The solutions for both $A_{1,n}$ and $A_{2,n}$ different from zero are

$$A_{1,n} = \pm\sqrt{\frac{(h_2\omega_{2,n}^2 - k_1\omega_{1,n}^2) - U^2(h_2\alpha_2 - k_1\alpha_1)}{h_1k_1 - h_2k_2}}, \tag{50a}$$

$$A_{2,n} = \pm\sqrt{\frac{(k_2\omega_{1,n}^2 - h_1\omega_{2,n}^2) - U^2(k_2\alpha_1 - h_1\alpha_2)}{h_1k_1 - h_2k_2}}, \tag{50b}$$

and they are defined only where both terms under the square root are positive.

For the case studied in section 6.2.2 with $B_{1,n} = A_{2,n} = 0$, equations (48) and (49) remain valid with $B_{2,n}$ replacing $A_{2,n}$; in contrast, equation (50) is replaced by

$$A_{1,n} = \pm\sqrt{\frac{(h_3\omega_{2,n}^2 - k_1\omega_{1,n}^2) - U^2(h_3\alpha_2 - k_1\alpha_1)}{h_1k_1 - h_3k_3}}. \tag{51a}$$

$$B_{2,n} = \pm\sqrt{\frac{(k_3\omega_{1,n}^2 - h_1\omega_{2,n}^2) - U^2(k_3\alpha_1 - h_1\alpha_2)}{h_1k_1 - h_3k_3}}. \tag{51b}$$

These analytical results are in excellent agreement with the numerical ones obtained by using the *Auto* software.

The case with companion mode participation for the Weaver and Unny model allows simple analytical solutions for divergence in the first longitudinal mode,

$$A_{1,n}^2 + B_{1,n}^2 = (\alpha_1 U^2 - \omega_{1,n}^2)/h_1, \quad A_{2,n}^2 + B_{2,n}^2 = 0, \tag{51a, b}$$

and for divergence in the second longitudinal mode,

$$A_{1,n}^2 + B_{1,n}^2 = 0, \quad A_{2,n}^2 + B_{2,n}^2 = (\alpha_2 U^2 - \omega_{2,n}^2)/k_1. \tag{52a, b}$$

Equations (51) and (52) prove that the post-divergence configurations, in the case of companion-mode participation, are described by surfaces generated by rotation of the divergence solution without companion mode around the V-axis; results of equation (51) are shown in Figure 9(a).

The axisymmetric solutions when all the degrees of freedom are active are given by

$$A_{1,n}^2 + B_{1,n}^2 = \frac{(h_2\omega_{2,n}^2 - k_1\omega_{1,n}^2) - U^2(h_2\alpha_2 - k_1\alpha_1)}{h_1k_1 - h_2k_2}, \tag{53a}$$

$$A_{2,n}^2 + B_{2,n}^2 = \frac{(k_2\omega_{1,n}^2 - h_1\omega_{2,n}^2) - U^2(k_2\alpha_1 - h_1\alpha_2)}{h_1k_1 - h_2k_2}, \tag{53b}$$

and by

$$A_{1,n}^2 + B_{1,n}^2 = \frac{(h_3\omega_{2,n}^2 - k_1\omega_{1,n}^2) - U^2(h_3\alpha_2 - k_1\alpha_1)}{h_1k_1 - h_3k_3}, \tag{54a}$$

$$A_{2,n}^2 + B_{2,n}^2 = \frac{(k_3\omega_{1,n}^2 - h_1\omega_{2,n}^2) - U^2(k_3\alpha_1 - h_1\alpha_2)}{h_1k_1 - h_3k_3}. \tag{54b}$$

Equations (53) are obtained by using the condition $B_{1,n}/A_{1,n} = -B_{2,n}/A_{2,n}$, which means that the first and second longitudinal modes are in anti-phase in θ, and equation (54) by using the condition $A_{1,n}/B_{1,n} = -B_{2,n}/A_{2,n}$, meaning that the first and second longitudinal modes are orthogonal in θ; these conditions are the only ones that allow axisymmetric solutions. It is to be noted that equations (53) admit solutions along a generating line of the axisymmetric surface; in contrast, equations (54) admit only helicoidal solutions, as a consequence of the condition $A_{1,n}/B_{1,n} = -B_{2,n}/A_{2,n}$ and the shape of the surfaces of equations (54a, b). The axisymmetric condition gives also two constraints for some of the coefficients in the equations of motion (45); they are: $h_2 - h_3 - h_4 = 0$ and $k_2 - k_3 - k_4 = 0$, and they are satisfied by the coefficients in equations (45) and (46).

Analytical solutions for the model of Païdoussis and Denise are complicated by the presence of three additional degrees of freedom. However, numerical solution of the algebraic equations is in excellent agreement with the solution obtained by using *Auto* in the case without companion mode participation. When the companion mode is considered, the post-divergence configurations are given by surfaces generated by rotation of the divergence solution without companion mode around the V-axis, as for the model of Weaver and Unny; this can easily be verified by using equations (46). Analogously to what was found in equations (53) and (54), the stationary solutions for the Païdoussis and Denise model are axisymmetric when they involve all the generalized co-ordinates and they satisfy the condition

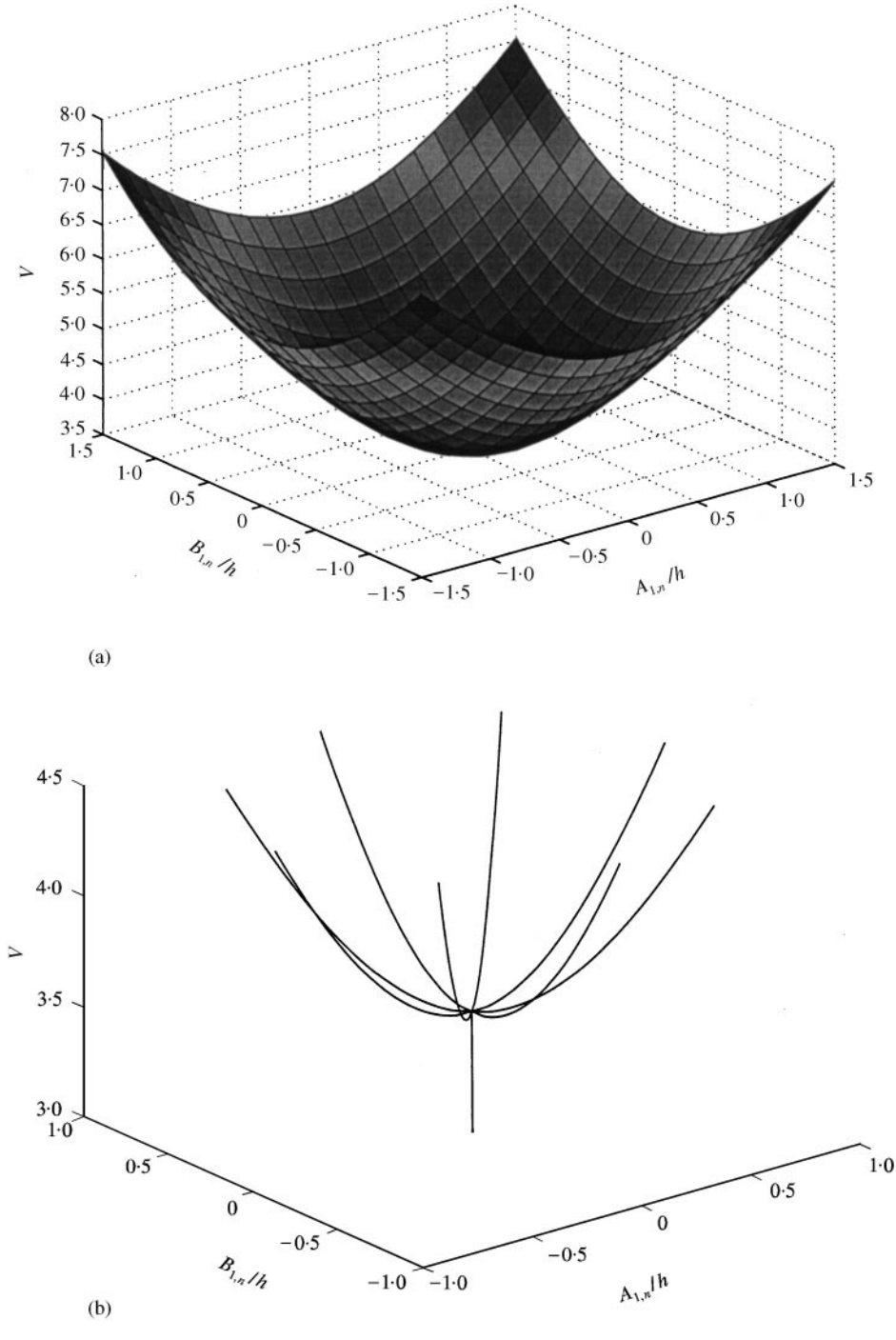

Figure 9. Divergence of the first longitudinal mode for the model of Weaver and Unny. (a) Analytical solution; (b) numerical solution starting from undisturbed initial conditions and different perturbations.

$B_{1,n}/A_{1,n} = -B_{2,n}/A_{2,n}$, i.e., when the first and second longitudinal modes are in anti-phase in θ (i.e. they are described by the same function in θ), or $A_{1,n}/B_{1,n} = -B_{2,n}/A_{2,n}$, i.e., when the first and second longitudinal modes are orthogonal in θ.

6.4. NON-LINEAR RESULTS WITH COMPANION-MODE PARTICIPATION

When all the generalized co-ordinates are retained in equations (45) and (46), the system does not possess a preferential angular co-ordinate to locate the modes. The solution can be imagined in three-dimensional (3-D) plots, where one represents the amplitude of the driven and companion modes versus V for the two pairs of variables $\{A_{1,n}, B_{1,n}\}$ and $\{A_{2,n}, B_{2,n}\}$. In particular, a section of this 3-D plot for zero amplitude of the companion mode ($B_{1,n} = 0$ and $B_{2n} = 0$ respectively) gives the 2-D plot already obtained in Figure 3 or 4; obviously, in view of the symmetry of the equations (for zero external excitation) and of the physical system, the same 2-D plot is obtained for a section at zero amplitude of the driven mode ($A_{1,n} = 0$ and $A_{2,n} = 0$ respectively). Therefore, the non-oscillatory solutions can be imagined as surfaces generated by rotation of the corresponding curves in Figure 3(a) [or Figures 3(b), 4(a) and (b), respectively] around the V-axis, as shown in section 6.3. Stable branches in Figures 3 and 4 generate stable surfaces. In this case, jumps from one point on the surface to another on the same surface or on a different surface can arise even more easily than for the case described in section 6.2. Moreover, the jumps can also give rise to the phenomenon of nodal lines travelling around the shell in the circumferential direction. Surfaces of rotation are obtained also when one represents in 3-D plots the solutions for the case studied in section 6.2.2 and represented in 2-D plots in Figures 7 and 8.

In order to simulate the dynamical behaviour of the complete system, equations (45) and (46) have been integrated numerically, starting from an initially undisturbed configuration at zero flow velocity. The adaptive step-size fourth- and fifth-order Runge–Kutta method has been used as the integration algorithm. Figure 9(b) shows the divergence of the first longitudinal mode for the Weaver and Unny model, starting from undisturbed initial conditions and different perturbations; it is clear that the bifurcation paths belong to the surface of revolution representing the stable solution. This confirms the result obtained in equation (51) and shown in Figure 9(a).

Figure 10 shows the dynamical behaviour of the system according to the model of Weaver and Unny, starting from an undisturbed initial condition and slowly increasing the flow velocity. The integration time is $10^6/\omega_{1,n}$ seconds and the number of integration points is 10 000. It is clear that the system remains in the initial configuration until divergence in the first mode, at $V = 3{\cdot}54$. At a flow velocity $V \approx 4{\cdot}76$, the system shows a transitional behaviour; after that, it diverges in the second longitudinal mode, with a corresponding modal change; between the two phases there is a relative rotation of the nodal lines around the shell. This result is in very good agreement with the results shown in Figure 7, where it is shown that the first-mode divergence loses stability at the same velocity. The oscillation

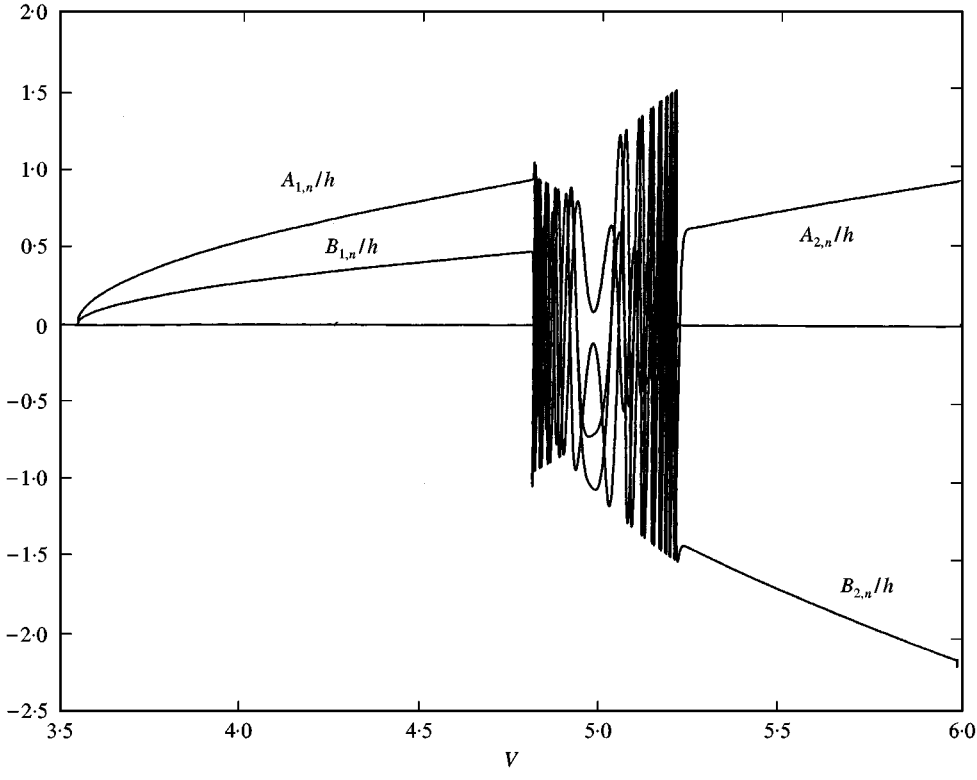

Figure 10. Behaviour of the system starting from undisturbed initial conditions and slowly increasing the non-dimensional flow velocity V for the model of Weaver and Unny.

amplitudes during the transitional state follow the shape of the stable branch "3" in Figure 7.

Figure 11 presents results of an analogous numerical integration of the equations of motion for the model of Païdoussis and Denise. Integration starts from a point on the first divergence mode ($B_{1,n} = A_{2,n} = B_{2,n} = 0$) and the flow velocity is slowly *decreased*; the integration time is $4{\cdot}3 \times 10^4/\omega_{1,n}$ seconds, and the number of integration points is 12 000. The behaviour of the system can easily be explained by comparison with Figure 4.

Several numerical integrations at a fixed velocity, $V = 4{\cdot}93$, have been performed starting with different initial conditions. Figure 12 shows a typical time history; all the generalized co-ordinates converge to different fixed points depending on the initial conditions. In particular, the generalized co-ordinates related to axisymmetric modes always converge to the same values; the relationships among the other generalized co-ordinates are plotted in Figure 13. In particular, Figures 13(a) and 13(b) show relationships analogous to equations (54a) and (54b), respectively, extended to the case with seven degrees of freedom, and Figure 13(c) shows that the system satisfies the relation $A_{1,n}/B_{1,n} = -B_{2,n}/A_{2,n}$. In Figure 13, dots represent results (fixed points) obtained with numerical integration; one of these results is shown in Figure 12.

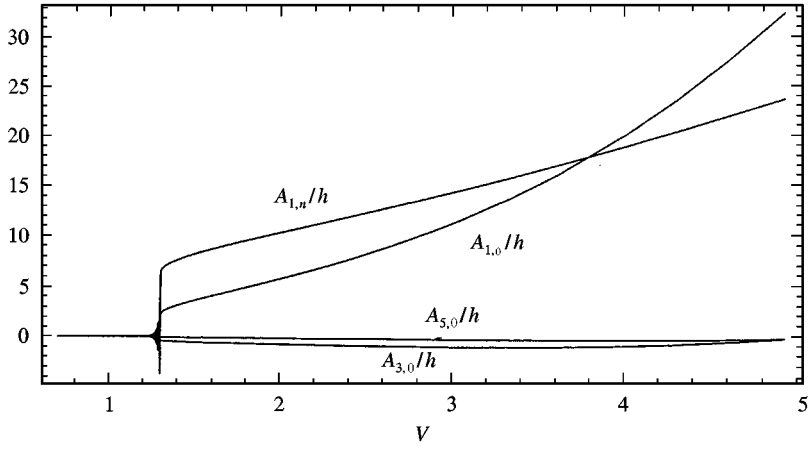

Figure 11. Behaviour of the system starting from a point on the first-divergence configuration and slowly decreasing the non-dimensional flow velocity V for the model of Païdoussis and Denise.

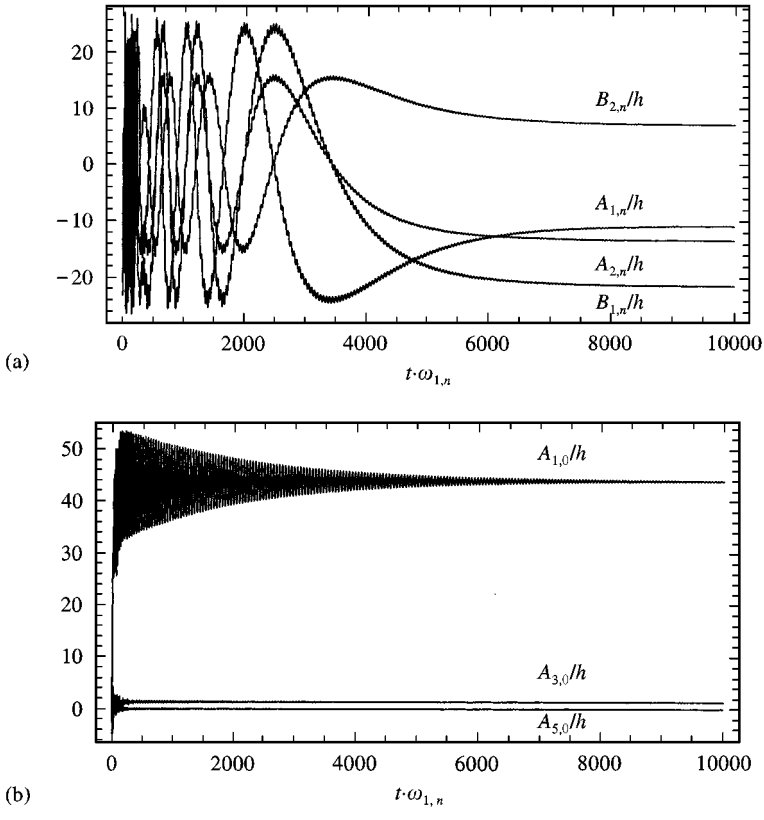

Figure 12. Numerical integration at a fixed velocity, $V = 4{\cdot}93$. (a) Generalized co-ordinates relative to asymmetric modes; (b) generalized co-ordinates relative to axisymmetric modes.

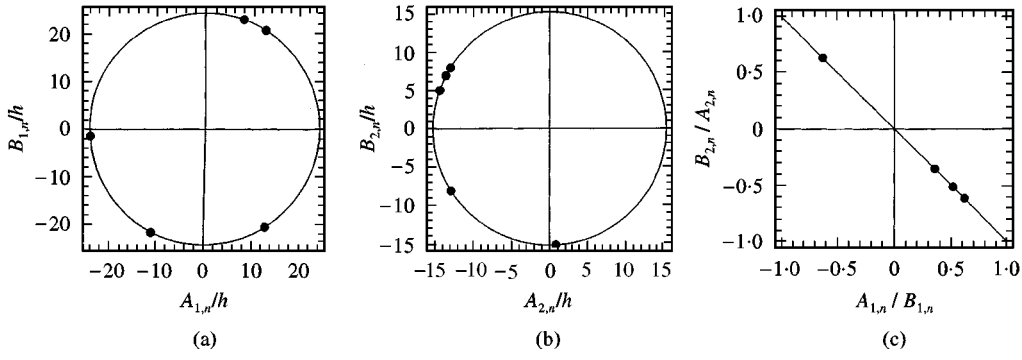

Figure 13. Relationship among the fixed points of the coupled-mode solution at velocity $V = 4{\cdot}93$. (a) Relationship between $A_{1,n}$ and $B_{1,n}$; (b) relationship between $A_{2,n}$ and $B_{2,n}$; (c) relationship between $A_{1,n}/B_{1,n}$ and $B_{2,n}/A_{2,n}$.

A numerical integration was performed starting from one of the fixed points obtained at $V = 4{\cdot}93$ and then slowly decreasing the flow velocity. The result is shown in Figure 14 and shows that all the seven generalized co-ordinates are different from zero for a large range of flow velocities. It is interesting to observe that, for $V > 1{\cdot}84$, the solution belongs to an axisymmetric surface and it is rotating around its axis; it gives a kind of helicoidal motion. This axisymmetric surface is obtained by rotation of branch "3" in Figure 8 around the V-axis. For $1{\cdot}31 < V < 1{\cdot}84$, the system follows the first-mode divergence without rotating any more. At $V = 1{\cdot}31$ the system gains the stable undeformed configuration. Figure 15 presents the shape of the shell in post-divergence configurations for the same branch (coupled-mode divergence) at $V = 2$, 3 and 4. One should note the twist of the shell and the growth in the post-divergence amplitudes with V.

Finally, a set of numerical integrations have been performed at flow velocity $V = 2$. Several initial conditions, of the form $A_{1,n} =$ constant have been tried, with the remaining variables and all the time derivatives equal to zero, to investigate the basin of attraction of first-mode divergence. Figure 16(a) shows the solution for the initial condition $A_{1,n} = 2{\cdot}5$, and it is seen that it converges to the undeformed condition. In contrast, the solution for the initial condition $A_{1,n} = 2{\cdot}6$ converges to the first-divergence branch, as shown in Figure 16(b). Thus, the lower bound of the basin of attraction for the stable first-mode divergence branch in terms of $A_{1,n}$ lies somewhere between $A_{1,n} = 2{\cdot}5$ and $2{\cdot}6$, which is actually a little lower than the unstable branch (which is at $A_{1,n} = 3{\cdot}5$).

7. DISCUSSION AND CONCLUSIONS

The present study clarifies for the first time several aspects of the dynamics and stability of simply supported circular cylindrical shells with flow, by means of non-linear theory. The results show that a circular cylindrical shell under the action of internal flow loses stability by divergence. The actual behaviour of the system, when axisymmetric modes are allowed shows that the divergence is subcritical,

giving a softening-type behaviour for small displacement, becoming hardening for larger amplitudes. It is very interesting to observe that the system has two or more stable solutions, related to divergence in the first or first and second longitudinal modes, much before linear divergence occurs. This means that the shell, if perturbed from the initial configuration, can have very severe deformations, which can be the cause of failure, much before the failure velocity predicted by the linear threshold. In particular, for the case studied, the system can diverge for V larger than 1·31, while linear theories predict divergence only for $V = 3{\cdot}33$, which represents a difference larger than 2·5 times! This means that a non-linear study is really necessary to predict stability of circular cylindrical shells containing flowing fluid. A synthesis of these non-linear results, compared to linear ones, is given in Table 1.

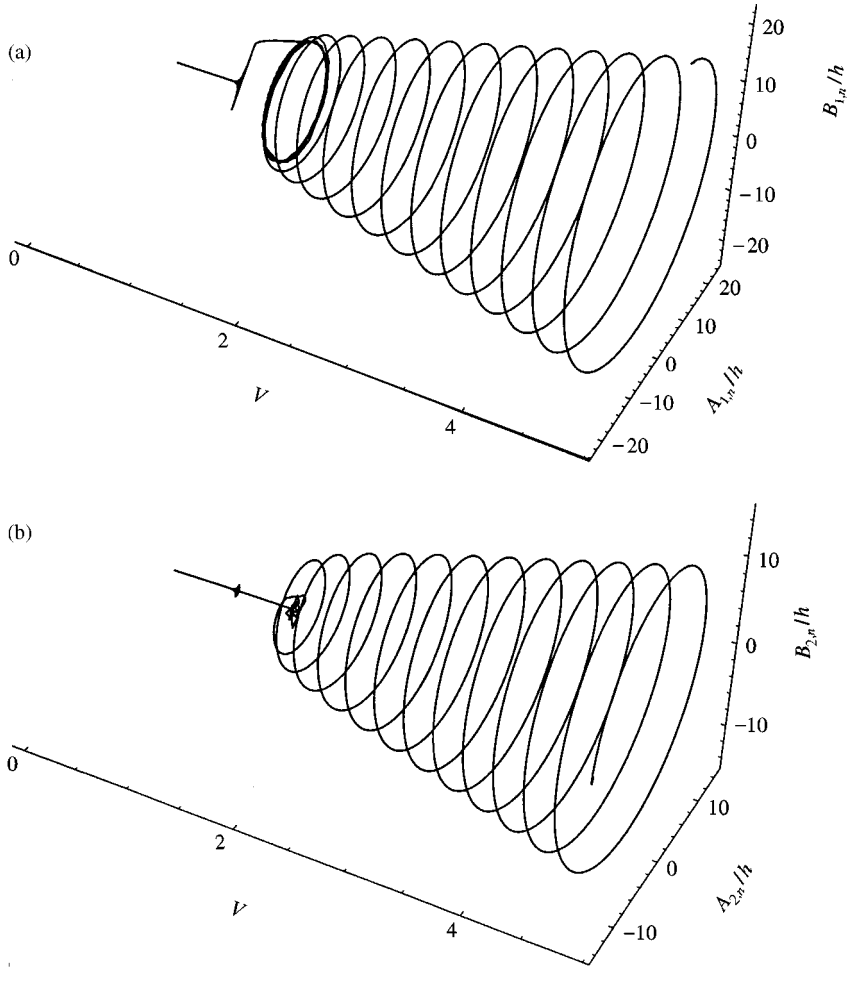

Figure 14. Behaviour of the system starting from a point on the coupled-mode divergence at $V = 4{\cdot}93$ obtained when slowly decreasing the non-dimensional flow velocity V; model of Païdoussis and Denise. Generalized co-ordinates: (a) $A_{1,n}$ and $B_{1,n}$ versus V; (b) $A_{2,n}$ and $B_{2,n}$ versus V; (c) $A_{1,0}$; (d) $A_{3,0}$; (e) $A_{5,0}$.

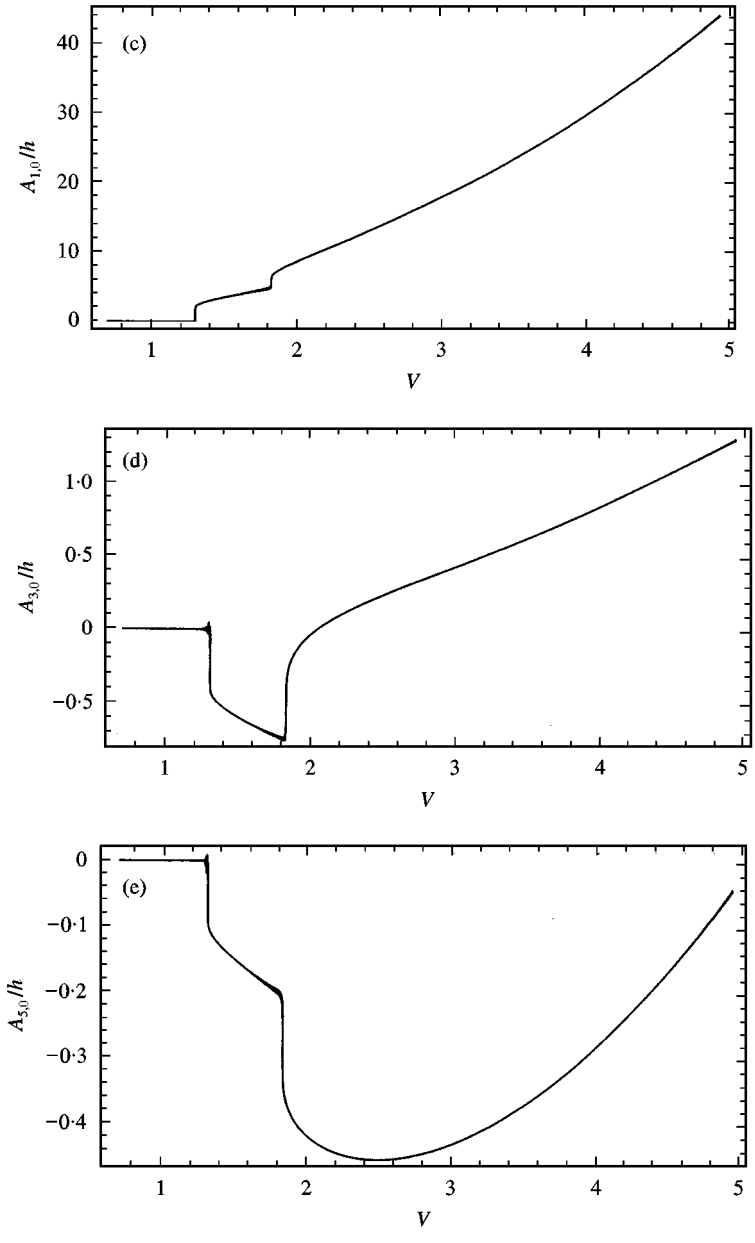

Figure 14. Continued.

Another important result is obtained for the coupled-mode divergence, which has been shown to be of two different kinds. In particular, it has been found that the first longitudinal mode combines (i) with the second longitudinal mode that is in anti-phase in the angular co-ordinate, and (ii) with the second longitudinal mode that is orthogonal to the first in the angular co-ordinate. These two solutions give rise to two quite distinct types of behaviour of the system.

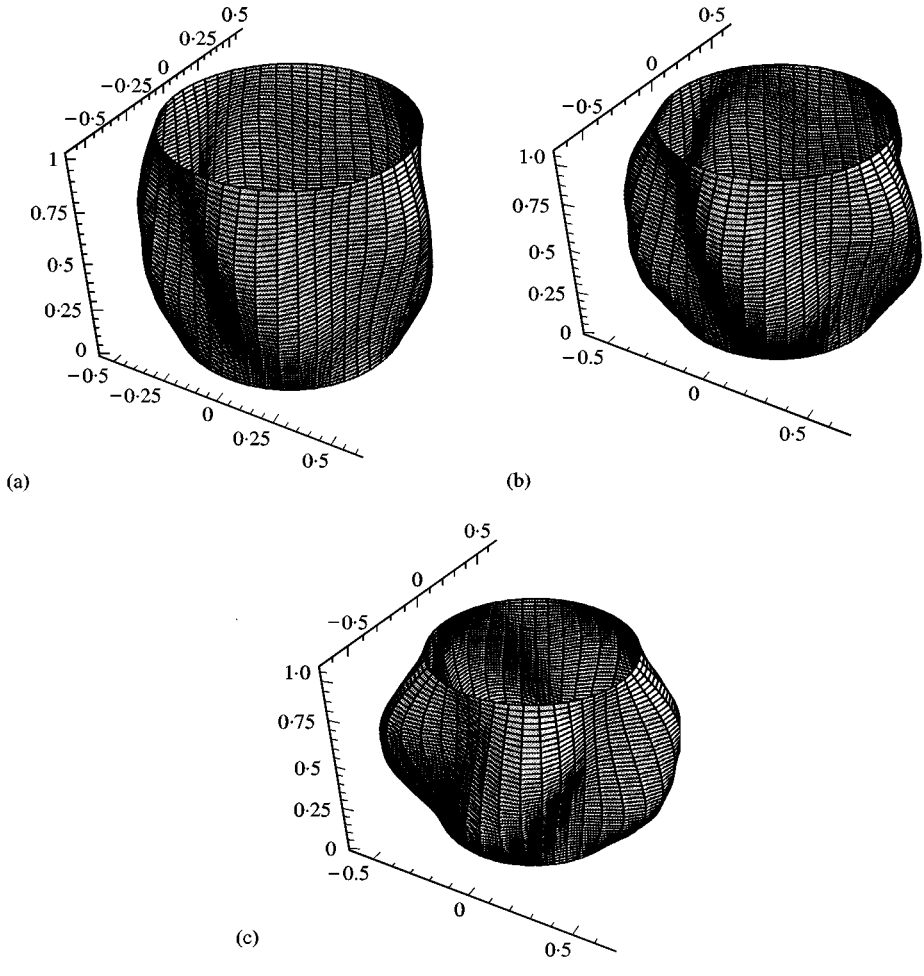

Figure 15. Shell shape for coupled-mode divergence at different flow velocities: (a) $V = 2$; (b) $V = 3$; (c) $V = 4$.

The present study could be improved by using a more refined non-linear shell theory instead of the non-linear Donnell shallow shell one. However, as a consequence of the system losing stability by divergence, the effect of neglecting in-plane inertia is negligible; more significant would be to use of a theory which is accurate for very large shell displacements. A non-linear theory to describe the fluid–structure interaction could be a further refinement, but this is expected to give a significant effect only at *very* large shell displacements. More interesting could be to verify the effect of additional longitudinal modes in the expansion of the shell flexural displacement that are expected to complicate further the post-divergence dynamics of the system; however, the solutions related to divergence in the first ($m = 1$) and second ($m = 2$) asymmetric modes, excluding coupled mode solutions, should remain unchanged. In fact, single-mode solutions should remain valid even if more asymmetric modes ($m > 2$) are added.

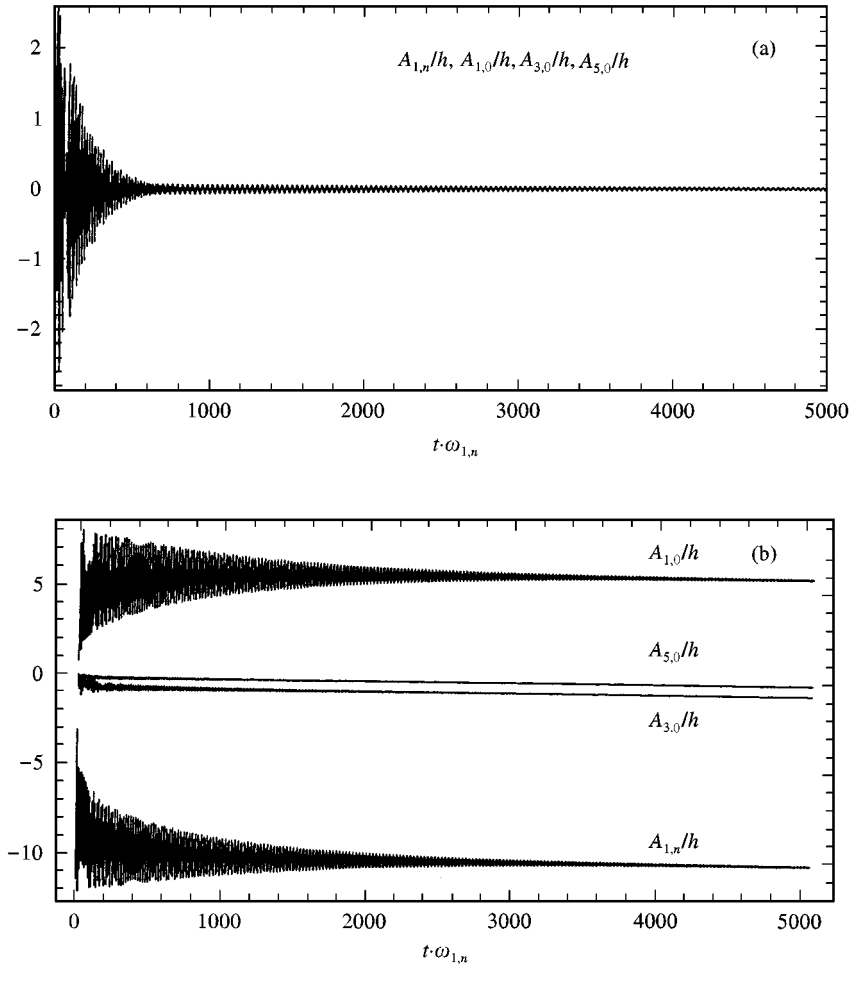

Figure 16. Numerical integration at $V = 2$ for Païdoussis and Denise model. Initial conditions different from zero: (a) $A_{1,n} = 2{\cdot}5$; (b) $A_{1,n} = 2{\cdot}6$.

TABLE 1

Comparison of linear and non-linear, non-dimensional critical fluid velocities V for the fluid–structure interaction model of Païdoussis and Denise

	First mode divergence	Second mode divergence	"Helicoidal" solution
Linear	$V = 3{\cdot}33$	$V = 4{\cdot}34$	—
Nonlinear	$1{\cdot}31 \leqslant V \leqslant 3{\cdot}33$	$1{\cdot}91 \leqslant V \leqslant 4{\cdot}34$	$V > 1{\cdot}84$

ACKNOWLEDGMENTS

The authors acknowledge the financial support of the Natural Sciences and Engineering Research Council of Canada, of Funds pour la Formation des Chercheurs et l'Aide à la Recherche of Québec and the Italian Space Agency.

REFERENCES

1. M. P. Païdoussis and J.-P. Denise 1972 *Journal of Sound and Vibration* **20**, 9–26. Flutter of thin cylindrical shells conveying fluid.
2. D. S. Weaver and T. E. Unny 1973 *Journal of Applied Mechanics* **40**, 48–52. On the dynamic stability of fluid-conveying pipes.
3. Y. Matsuzaki and Y. C. Fung 1977 *Journal of Sound and Vibration* **54**, 317–330. Unsteady fluid dynamic forces on a simply-supported circular cylinder of finite length conveying a flow, with applications to stability analysis.
4. M. P. Païdoussis, S. P. Chan and A. K. Misra 1984 *Journal of Sound and Vibration* **97**, 201–235. Dynamics and stability of coaxial cylindrical shells containing flowing fluid.
5. M. P. Païdoussis, A. K. Misra and S. P. Chan 1985 *Journal of Applied Mechanics* **52**, 389–396. Dynamics and stability of coaxial cylindrical shells conveying viscous fluid.
6. E. H. Dowell 1966 *AIAA Journal* **4**, 1267–1275. Nonlinear oscillations of a fluttering plate.
7. E. H. Dowell 1967 *AIAA Journal* **5**, 1856–1862. Nonlinear oscillations of a fluttering plate; II.
8. E. H. Dowell 1969 *AIAA Journal* **7**, 424–431. Nonlinear flutter of curved plates.
9. E. H. Dowell 1970 *AIAA Journal* **8**, 259–261. Nonlinear flutter of curved plates, II.
10. L. Morino, C. C. Kuo and J. Dugundji 1972 *AIAA Journal* **10**, 1479–1484. Perturbation and harmonic balance methods for nonlinear panel flutter.
11. M. P. Païdoussis, 1998 *Fluid–Structure Interactions*: *Slender Structures and Axial Flow*, Vol. 1. London, UK: Academic Press.
12. M. D. Olson and Y. C. Fung 1967 *AIAA Journal* **5**, 1849–1856. Comparing theory and experiment for the supersonic flutter of circular cylindrical shells.
13. D. A. Evensen and M. D. Olson 1967 *NASA TN D*-4265. Nonlinear flutter of a circular cylindrical shell in supersonic flow.
14. D. A. Evensen and M. D. Olson 1968 *AIAA Journal* **6**, 1522–1527. Circumferentially travelling wave flutter of a circular cylindrical shell.
15. D. A. Evensen 1967 *NASA TN D*-4090. Nonlinear flexural vibrations of thin-walled circular cylinders.
16. J. H. Ginsberg 1973 *Journal of Applied Mechanics* **40**, 471–477. Large amplitude forced vibrations of simply supported thin cylindrical shells.
17. J. C. Chen and C. D. Babcock 1975 *AIAA Journal* **13**, 868–876. Nonlinear vibration of cylindrical shells.
18. M. Amabili, F. Pellicano and M. P. Païdoussis 1998 *Journal of Fluids and Structures* **12**, 883–918. Nonlinear vibrations of simply supported, circular cylindrical shells, coupled to quiescent fluid.
19. U. Olsson 1978 *AIAA Journal* **16**, 360–362. Supersonic flutter of heated circular cylindrical shells with temperature-dependent material properties.
20. A. A. Lakis and A. Laveau 1991 *International Journal of Solids and Structures* **28**, 1079–1094. Non-linear dynamic analysis of anisotropic cylindrical shells containing a flowing fluid.
21. A. Selmane and A. A. Lakis 1997 *Journal of Sound and Vibration* **202**, 67–93. Non-linear dynamic analysis of orthotropic open cylindrical shells subjected to a flowing fluid.
22. P. B. Gonçalves and R. C. Batista 1988 *Journal of Sound and Vibration* **127**, 133–143. Non-linear vibration analysis of fluid-filled cylindrical shells.
23. M. Ganapathi and T. K. Varadan 1996 *Journal of Sound and Vibration* **192**, 1–14. Large amplitude vibrations of circular cylindrical shells.
24. E. H. Dowell and C. S. Ventres 1968 *International Journal of Solids and Structures* **4**, 975–991. Modal equations for the nonlinear flexural vibrations of a cylindrical shell.
25. S. Atluri 1972 *International Journal of Solids and Structures* **8**, 549–569. A perturbation analysis of non-linear free flexural vibrations of a circular cylindrical shell.

26. J. H. Ginsberg 1975 *Journal of Sound and Vibration* **40**, 359–379. Multi-dimensional non-linear acoustic wave propagation. Part II: the non-linear interaction of an acoustic fluid and plate under harmonic excitation.
27. D. G. Randall 1958 *Ames Research Center* (*NASA*) *Report*, *ARC R. and M. No.* 3067. Supersonic flow past quasi-cylindrical bodies of almost circular cross-section.
28. F. I. N. Niordson 1953 *Transactions of the Royal Institute of Technology*, *Stockholm*, *Sweden*, *No.* 73. Vibrations of cylindrical tube containing flowing fluid.
29. S. Wolfram 1996 *The Mathematica Book*. Cambridge, UK: Cambridge University Press, third edition.
30. P. J. Holmes 1978 *Journal of Applied Mechanics* **45**, 619–622. Pipes supported at both ends cannot flutter.
31. M. Amabili 1996 *Journal of Sound and Vibration* **191**, 757–780. Free vibration of partially filled, horizontal cylindrical shells.
32. E. J. Doedel and J. P. Kernéves 1986 *Applied Mathematics Report*, *California Institute of Technology*, *Pasadena*, *California*, *U.S.A.* Auto: software for continuation and bifurcation problems in ordinary differential equations. (obtainable from doedel@cs.concordia.ca).

APPENDIX A: TIME FUNCTIONS USED IN EQUATION (33)

The functions $c_i(t)$, $i = 1, \ldots, 33$, used in equation (33) are given by

$$c_1(t) = A_{1,n}(t)\,\frac{Eh\pi^2}{L^2R}\Big/\left(\frac{\pi^2}{L^2}+\frac{n^2}{R^2}\right)^2, \qquad c_2(t) = B_{1,n}(t)\,\frac{Eh\pi^2}{L^2R}\Big/\left(\frac{\pi^2}{L^2}+\frac{n^2}{R^2}\right)^2, \tag{A1, A2}$$

$$c_3(t) = A_{2,n}(t)\,\frac{4Eh\pi^2}{L^2R}\Big/\left(\frac{4\pi^2}{L^2}+\frac{n^2}{R^2}\right)^2, \qquad c_4(t) = B_{2,n}(t)\frac{4Eh\pi^2}{L^2R}\Big/\left(\frac{4\pi^2}{L^2}+\frac{n^2}{R^2}\right)^2, \tag{A3, A4}$$

$$c_5(t) = A_{1,0}(t)\,\frac{EhL^2}{\pi^2R}, \qquad c_6(t) = A_{3,0}(t)\,\frac{EhL^2}{9\pi^2R}, \tag{A5, A6}$$

$$c_7(t) = A_{5,0}(t)\,\frac{EhL^2}{25\pi^2R}, \qquad c_8(t) = -\left(A_{1,n}(t)A_{2,n}(t) + B_{1,n}(t)B_{2,n}(t)\right)\frac{Ehn^2L^2}{4\pi^2R^2}, \tag{A7, A8}$$

$$c_9(t) = \left(A_{1,n}^2(t) + B_{1,n}^2(t)\right)\frac{Ehn^2L^2}{32\pi^2R^2}, \tag{A9}$$

$$c_{10}(t) = \left(A_{1,n}(t)A_{2,n}(t) + B_{1,n}(t)B_{2,n}(t)\right)\frac{Ehn^2L^2}{36\pi^2R^2}, \tag{A10}$$

$$c_{11}(t) = \left(A_{2,n}^2(t) + B_{2,n}^2(t)\right)\frac{Ehn^2L^2}{128\pi^2R^2}, \qquad c_{12}(t) = -A_{1,n}(t)A_{1,0}(t)\,\frac{Eh\pi^2R^2}{2L^2n^2}, \tag{A11, A12}$$

$$c_{13}(t) = -A_{2,n}(t)(A_{1,0}(t) + 9A_{3,0}(t))\,\frac{Ehn^2\pi^2}{2L^2R^2}\Big/\left(\frac{\pi^2}{L^2}+\frac{n^2}{R^2}\right)^2, \tag{A13}$$

$$c_{14}(t) = A_{1,n}(t)(A_{1,0}(t) - 9A_{3,0}(t))\,\frac{Ehn^2\pi^2}{2L^2R^2}\Big/\left(\frac{4\pi^2}{L^2}+\frac{n^2}{R^2}\right)^2, \tag{A14}$$

$$c_{15}(t) = A_{2,n}(t)(A_{1,0}(t) - 25A_{5,0}(t))\,\frac{Ehn^2\pi^2}{2L^2R^2}\Big/\left(\frac{9\pi^2}{L^2}+\frac{n^2}{R^2}\right)^2, \tag{A15}$$

$$c_{16}(t) = A_{1,n}(t)(9A_{3,0}(t) - 25A_{5,0}(t))\,\frac{Ehn^2\pi^2}{2L^2R^2}\Big/\left(\frac{16\pi^2}{L^2}+\frac{n^2}{R^2}\right)^2, \tag{A16}$$

$$c_{17}(t) = 9A_{2,n}(t)A_{3,0}(t)\,\frac{Ehn^2\pi^2}{2L^2R^2}\Big/\left(\frac{25\pi^2}{L^2}+\frac{n^2}{R^2}\right)^2, \tag{A17}$$

$$c_{18}(t) = 25A_{1,n}(t)A_{5,0}(t)\,\frac{Ehn^2\pi^2}{2L^2R^2}\Big/\left(\frac{36\pi^2}{L^2}+\frac{n^2}{R^2}\right)^2, \tag{A18}$$

$$c_{19}(t) = 25A_{2,n}(t)A_{5,0}(t)\,\frac{Ehn^2\pi^2}{2L^2R^2}\Big/\left(\frac{49\pi^2}{L^2}+\frac{n^2}{R^2}\right)^2, \tag{A19}$$

$$c_{20}(t) = -B_{1,n}(t)A_{1,0}(t)\,\frac{Eh\pi^2R^2}{2L^2n^2}, \tag{A20}$$

$$c_{21}(t) = -B_{2,n}(t)(A_{1,0}(t) + 9A_{3,0}(t))\,\frac{Ehn^2\pi^2}{2L^2R^2}\Big/\left(\frac{\pi^2}{L^2}+\frac{n^2}{R^2}\right)^2, \tag{A21}$$

$$c_{22}(t) = B_{1,n}(t)(A_{1,0}(t) - 9A_{3,0}(t))\,\frac{Ehn^2\pi^2}{2L^2R^2}\Big/\left(\frac{4\pi^2}{L^2}+\frac{n^2}{R^2}\right)^2, \tag{A22}$$

$$c_{23}(t) = B_{2,n}(t)(A_{1,0}(t) - 25A_{5,0}(t))\,\frac{Ehn^2\pi^2}{2L^2R^2}\Big/\left(\frac{9\pi^2}{L^2}+\frac{n^2}{R^2}\right)^2, \tag{A23}$$

$$c_{24}(t) = B_{1,n}(t)(9A_{3,0}(t) - 25A_{5,0}(t))\,\frac{Ehn^2\pi^2}{2L^2R^2}\Big/\left(\frac{16\pi^2}{L^2}+\frac{n^2}{R^2}\right)^2, \tag{A24}$$

$$c_{25}(t) = 9B_{2,n}(t)A_{3,0}(t)\,\frac{Ehn^2\pi^2}{2L^2R^2}\Big/\left(\frac{25\pi^2}{L^2}+\frac{n^2}{R^2}\right)^2, \tag{A25}$$

$$c_{26}(t) = 25B_{1,n}(t)A_{5,0}(t)\,\frac{Ehn^2\pi^2}{2L^2R^2}\Big/\left(\frac{36\pi^2}{L^2}+\frac{n^2}{R^2}\right)^2, \tag{A26}$$

$$c_{27}(t) = 25B_{2,n}(t)A_{5,0}(t)\,\frac{Eh n^2\pi^2}{2L^2R^2}\Big/\left(\frac{49\pi^2}{L^2}+\frac{n^2}{R^2}\right)^2, \tag{A27}$$

$$c_{28}(t) = (-A_{1,n}^2(t) + B_{1,n}^2(t) - 4A_{2,n}^2(t) + 4B_{2,n}^2(t))\,\frac{Eh\pi^2R^2}{32L^2n^2}, \tag{A28}$$

$$c_{29}(t) = -9(A_{1,n}(t)A_{2,n}(t) - B_{1,n}(t)B_{2,n}(t))\,\frac{Eh\pi^2n^2}{4L^2R^2}\Big/\left(\frac{\pi^2}{L^2}+\frac{4n^2}{R^2}\right)^2, \tag{A29}$$

$$c_{30}(t) = (A_{1,n}(t)A_{2,n}(t) - B_{1,n}(t)B_{2,n}(t))\,\frac{Eh\pi^2n^2}{4L^2R^2}\Big/\left(\frac{9\pi^2}{L^2}+\frac{4n^2}{R^2}\right)^2, \tag{A30}$$

$$c_{31}(t) = -(A_{1,n}(t)B_{1,n}(t) + 4A_{2,n}(t)B_{2,n}(t))\,\frac{Eh\pi^2R^2}{16L^2n^2}, \tag{A31}$$

$$c_{32}(t) = -9(A_{1,n}(t)B_{2,n}(t) + A_{2,n}(t)B_{1,n}(t))\,\frac{Eh\pi^2n^2}{4L^2R^2}\Big/\left(\frac{\pi^2}{L^2}+\frac{4n^2}{R^2}\right)^2, \tag{A32}$$

$$c_{33}(t) = (A_{1,n}(t)B_{2,n}(t) + A_{2,n}(t)B_{1,n}(t))\,\frac{Eh\pi^2n^2}{4L^2R^2}\Big/\left(\frac{9\pi^2}{L^2}+\frac{4n^2}{R^2}\right)^2. \tag{A33}$$

APPENDIX B: CONTINUITY OF CIRCUMFERENTIAL DISPLACEMENT

In this Appendix B, it is proved that the continuity condition of the circumferential displacement v is satisfied exactly by the assumed mode expansion. This continuity condition is given by

$$\int_0^{2\pi}\frac{\partial v}{\partial\theta}\,\mathrm{d}\theta = v(2\pi) - v(0) = 0. \tag{B1}$$

For both of the two constraints considered at the shell ends, by using equations (3–5), equation (B1) is transformed into

$$\int_0^{2\pi}\left[\frac{1}{Eh}\left(\frac{\partial^2F}{\partial x^2} - \nu\,\frac{\partial^2F}{R^2\partial\theta^2}\right) + \frac{w}{R} - \frac{1}{2}\left(\frac{\partial w}{R\partial\theta}\right)^2\right]\mathrm{d}\theta = 0. \tag{B2}$$

The terms involved in equation (B2), after some calculations, are

$$\frac{1}{Eh}\int_0^{2\pi}\frac{\partial^2F}{\partial x^2}\,\mathrm{d}\theta = \frac{2\pi}{Eh}\,\bar{N}_\theta + \frac{4}{R}\left(A_{1,0}(t) + \frac{A_{3,0}(t)}{3} + \frac{A_{5,0}(t)}{5}\right)$$

$$-\frac{2\pi}{R}\left[A_{1,0}(t)\sin(\pi x/L) + A_{3,0}(t)\sin(3\pi x/L) + A_{5,0}(t)\sin(5\pi x/L)\right]$$

$$-\frac{\pi n^2}{R^2}\Bigg[-\frac{A_{1,n}(t)A_{2,n}(t)+B_{1,n}(t)B_{2,n}(t)}{2}\cos(\pi x/L)$$

$$+\frac{A_{1,n}^2(t)+B_{1,n}^2(t)}{4}\cos(2\pi x/L)+\frac{A_{1,n}(t)A_{2,n}(t)+B_{1,n}(t)B_{2,n}(t)}{2}\cos(3\pi x/L)$$

$$+\frac{A_{2,n}^2(t)+B_{2,n}^2(t)}{4}\cos(4\pi x/L)\Bigg], \tag{B3}$$

$$\frac{1}{Eh}\int_0^{2\pi}\frac{\partial^2 F}{R^2\partial\theta^2}\,\mathrm{d}\theta=\frac{2\pi}{Eh}\bar{N}_x, \tag{B4}$$

$$\frac{1}{Eh}\int_0^{2\pi}\frac{w}{R}\,\mathrm{d}\theta=\frac{2\pi}{EhR}\left[A_{1,0}(t)\sin(\pi x/L)+A_{3,0}(t)\sin(3\pi x/L)\right.$$

$$\left.+A_{5,0}(t)\sin(5\pi x/L)\right], \tag{B5}$$

$$\frac{1}{Eh}\int_0^{2\pi}\left(\frac{\partial w}{R\partial\theta}\right)^2\mathrm{d}\theta=\frac{\pi n^2}{EhR^2}\left\{(A_{1,n}^2(t)+B_{1,n}^2(t))\left[\frac{1-\cos(2\pi x/L)}{2}\right]\right.$$

$$+(A_{2,n}^2(t)+B_{2,n}^2(t))\left[\frac{1-\cos(4\pi x/L)}{2}\right]+(A_{1,n}(t)A_{2,n}(t)$$

$$\left.+B_{1,n}(t)B_{2,n}(t))[\cos(\pi x/L)-\cos(3\pi x/L)]\right\}, \tag{B6}$$

and, again for both the boundary conditions $N_x=0$ and $u=0$,

$$\bar{N}_\theta-\nu\bar{N}_x=Eh\Bigg[-\frac{2}{\pi R}\left(A_{1,0}(t)+A_{3,0}(t)+A_{5,0}(t)\right)+\frac{n^2}{8R^2}(A_{1,n}^2(t)$$

$$+B_{1,n}^2(t)+A_{2,n}^2(t)+B_{2,n}^2(t))\Bigg]. \tag{B7}$$

Upon substituting equations (B3–B7) into equation (B2), it is found that the left-hand side of this equation is identically zero for all x values. This proves that the continuity condition is exactly satisfied.